

Copyright © 2017, Paper 00-000; 000 words, 14 Figures, 0 Animations, 0 Tables.  
<http://EarthInteractions.org>

# A Model-Based Assessment of Potential Impacts of Man-Made Reservoirs on Precipitation

**Jesse Winchester, Rezaul Mahmood,<sup>a</sup> and William Rodgers**

Meteorology Program, Department of Geography and Geology and Kentucky Climate Center, Western Kentucky University, Bowling Green, Kentucky

**Faisal Hossain**

Department of Civil and Environmental Engineering, University of Washington, Seattle, Washington

**Eric Rappin**

Meteorology Program, Department of Geography and Geology and Kentucky Climate Center, Western Kentucky University, Bowling Green, Kentucky

**Joshua Durkee**

Meteorology Program, and CHAOS Laboratory, Department of Geography and Geology, Western Kentucky University, Bowling Green, Kentucky

**Themis Chronis**

Earth System Science Center, University of Alabama in Huntsville, Huntsville, Alabama

Received 17 May 2016; in final form 15 July 2017

**AU2**

<sup>a</sup> Corresponding author: Rezaul Mahmood, [xxxxxxx@wku.edu](mailto:xxxxxxx@wku.edu)

DOI: 10.1175/EI-D-16-0016.1

**ABSTRACT:** Land-use land-cover change (LULCC) plays an important role in weather and climate systems. Human modifications of land cover include building reservoirs and thus creating artificial lakes for multipurpose use. In this research, the authors have completed a Weather Research and Forecasting (WRF) Model assessment of impacts of two large parallel lakes on precipitation. This area is located in the western part of the states of Kentucky and Tennessee and known as the Land between the Lakes (LBL). To determine the impacts, this study has replaced the lakes with grass, deciduous forests, and bare soil and conducted model simulations for three precipitation events of different magnitudes.

The analysis suggests that precipitation increased in some cases and reduced in others. One of the key impacts of LULCC in the LBL area is the relocation of precipitation cells and also the timing of precipitation. Local precipitation amounts increased or decreased with these relocations. In summary, establishment of lakes or replacement of lakes with alternate land cover may modify local precipitation in the LBL area.

**AUT**

**KEYWORDS:** Anthropogenic effects; Atmosphere-land interaction; Land use; Local effects

## 1. Introduction and background

Land-use land-cover change (LULCC) plays an important role in modulating weather and climate at all spatiotemporal scales (Pielke et al. 2011; Mahmood et al. 2014). Relationships between land cover and the atmosphere have been well studied in terms of their influence on weather and climate (Halldin et al. 1999; Narisma et al. 2003; Schneider and Eugster 2005; Adegoke et al. 2007; Pielke et al. 2007). Observational data have revealed the strong influence of vegetation on the distribution of surface fluxes and moisture (Smith et al. 1994; Adegoke et al. 2007; Mengelkamp et al. 2006; Betts et al. 2007; LeMone et al. 2007). Furthermore, modeling studies have also demonstrated the influence of LULCC and soil moisture on the land surface–atmospheric interactions (Chang and Wetzel 1991; Clark and Arritt 1995; Pielke 2001; Mahmood and Hubbard 2002; Adegoke et al. 2003; McPherson and Stensurd 2005; Gero and Pitman 2006; Frye and Mote 2010; Mahmood et al. 2011; Leeper et al. 2011; Suarez et al. 2014). Changes in surface heating and evapotranspiration (ET) rates over a heterogeneous land cover can give rise to thermal/density gradients at the surface that are large enough to organize the planetary boundary layer (PBL) wind fields into mesoscale circulations (Smith et al. 1994).

LULCC-related atmospheric response also affects convection and precipitation (cf. Chen and Avissar 1994; Carleton et al. 2001; Pielke 2001; Nair et al. 2011; Sen Roy et al. 2011). The current study investigates the effects of Kentucky Lake and Lake Barkley [also known as the Land between the Lakes (LBL)] on selected precipitation events using the Weather Research and Forecasting (WRF) Model (Figure 1). This is the second part of an exploratory and observational data-based research by Durkee et al. (2014) where 12 precipitation events around the LBL region of Kentucky and Tennessee were investigated. They have found both enhanced and diminished convection in the LBL area as storms passed (Durkee et al. 2014).

**F1**

To further understand the influence of the LBL and LULCC, this study considered potential changes/replacement of the lakes to grassland, broadleaf



Figure 1. Rectangular bounds of (a) the outer domain, (b) the inner domain, and (c) the LBL area.

deciduous forest, and bare soil and its impacts on precipitation. Subsequently, this research applied the WRF Model for three precipitation events under these land-cover scenarios and analyzed subsequent changes in precipitation. Simulations/experiments of this type allow improved identification of the possible influences on local precipitation patterns surrounding the LBL area with regard to the changes in land cover.

The LBL area is located in western part of the Kentucky–Tennessee state borders and is characterized by two artificial lakes (Kentucky Lake and Lake Barkley) that are parallel and encompassing an area of 680 km<sup>2</sup> (Figure 1; Durkee et al. 2014). These artificial lakes were developed over the Tennessee (Kentucky Lake) and Cumberland Rivers (Lake Barkley). Since the establishment of the lakes in 1950s, anecdotal data suggest notable change in precipitation patterns in the area.

Conceptually, this precipitation modification has merit because from west to east, the LBL area can be viewed as intermittent boundaries of land–water. As a result, it provides an additional moisture source (higher evapotranspiration/latent energy flux, lower Bowen ratio), surface roughness heterogeneity (vegetation vs water), an environment for differential heating, and land surface discontinuity. The combination of these factors can play an important role in generating mesoscale



circulations and initiating deep convection (Ookouchi et al. 1984; Yan and Anthes 1988; Chen and Avissar 1994; Segal and Arritt 1992; Weaver and Avissar 2001; McPherson et al. 2004; McPherson 2007; Mahmood et al. 2011).

Jacquot (2009) noted that there are approximately 845 000 dams and artificial reservoirs around the world and their total surface area is about 33% of the total freshwater surface area of the globe. It is reported by Bates et al. (2008) that there has been a continual increase in dam construction in developing countries and is projected to continue in the foreseeable future as demand for water and energy increases. Although several studies explored the impact of large reservoirs on hydroclimatology, Durkee et al. (2014) is one of the few who investigated the modification of precipitating systems at the meteorological time scale. The majority of the recent studies on artificial reservoirs have focused on precipitation modification on the climate scale. For example, Degu et al. (2011) assessed the impacts of 92 large dams and noted that the modifications were mostly for summer precipitation over Mediterranean, semiarid, and arid climates. In a subsequent study, Degu and Hossain (2012) analyzed climate data and found increased moistening of the boundary layer by 5%–15% over areas downwind of dams in arid/semiarid regions during summer. Hence, an additional benefit of this study is the advancement of understanding of the impacts of large reservoirs on local precipitation.

At meteorological scales, most studies have involved the use of more physical-based models rather than observational records. For example, Gangoiti et al. (2011) developed a method for estimating evaporative source regions for heavy precipitation in the Mediterranean part of Europe using backtrajectory analysis. Eltahir (1989) investigated a possible feedback mechanism for the annual rainfall in Bahr el Ghazal Basin in Sudan due to open water evaporation. In another study, Kunstmann and Knoche (2011) used a regional atmospheric model to understand the contribution of moisture by Lake Volta in Ghana to precipitation that occurred downwind. Results from these studies found that up to 8% of precipitation have their sources from artificial lake evaporation. These studies provide an insightful basis for further exploring the modification of storms that is ascribed to LULCCs that occur after the construction of artificial reservoirs using numerical modeling of the land–atmosphere interaction. As previously highlighted, this is a follow-up observational study where we employ the WRF Model for three selected precipitation events to assess the impacts of the LBL. We have replaced lake water bodies with grassland (GRAS), broadleaf deciduous forest (FORE), and bare soil (BARE) and for a total of 12 simulations [ $3 \text{ LULCC} \times 3 \text{ precipitation events} = 9 + 3 \text{ control simulations (CTRL)} = 12$ ]. Subsequently, precipitation and related parameters were investigated to better understand modification of precipitation and land surface–atmosphere interactions associated with the LBL and LULCC.

The key research question is as follows: Does the presence of the two run-on-river reservoirs and the surrounding LULCC modify precipitation in the region? During the assessment of this question we would investigate potential changes in precipitation amount and the displacement of precipitation cells. The potential changes in precipitation totals may include increase or decrease associated with a particular type of modified LULC. In other words, replacement of the lakes with various land-cover types may not necessarily linearly decrease total precipitation. However, they may rather result in changes in the locations of precipitation.

The pursuit of the above goal is critical from the standpoint of water sustainability in a changing climate and increasing water demand from population growth. To meet future demand for water and energy, the construction of numerous large dams has also been proposed as a key solution (Graf 1999). For instance, the Southeastern Anatolia (GAP) dam and irrigation project in Turkey, the Itaipu hydroelectric dam located on the border between Brazil and Paraguay, the Three Gorges Dam (TGD) hydropower project in China, and the Grand Ethiopian Renaissance (GER) hydroelectric dam on Blue Nile River, Ethiopia, are some recent examples to alleviate water and energy shortages. It is clear that rising water demand and pressures or urbanization will result in the continuation of current large reservoirs (in the developed world) or the construction of new ones (in developing world). Understanding the postconstruction weather impacts of the land-use changes, made possible with numerical modeling, can help us understand the various land-use options for sustainability planning and its impact on precipitation.

The following sections include a brief description of the model, experimental design, results and discussions, and conclusions.

## 2. Methodology

### 2.1. The model

This study used the WRF Model version 3.4.1 (NCAR 2012). This model includes a series of microphysics, cumulus parameterization, PBL, surface layer, land surface model, radiation, and turbulent scheme options. The selection of physics options for this study were based on previous similar experiments conducted by the authors for this region (e.g., Quintanar et al. 2008, 2009, 2012; Leeper et al. 2011; Mahmood et al. 2011; Sarriz et al. 2014). For this sensitivity analysis, the Noah land surface model (Chen and Dudhia 2001a,b) was used, which includes vegetation parameters such as stomatal resistance, roughness length, leaf area index, and root depth for the simulation of surface moisture and energy budgets. The Noah LSM considers four soil layers with depths of 0.1, 0.3, 0.6, and 1 m with a reservoir beyond 1 m and soil physical properties including heat capacity, wilting point, and hydraulic conductivity. It determines the movement of moisture through the soil by gravitation pull, capillarity action, and transpiration.

The Yonsei University scheme (Hong 2010) for the PBL and Kain–Fritsch scheme for cumulus parameterization were selected for simulations (Kain 2004). In addition, it used WRF single-moment 6-class scheme for microphysics (Hong and Lim 2006) and the Rapid Radiative Transfer Model for GCMs (RRTMG) scheme for longwave and shortwave radiation (Iacono et al. 2008). This scheme provides detailed treatment of various gaseous constituents of the atmosphere for shortwave and longwave radiation.

The PBL scheme involves simulation of boundary layer fluxes, mixing of air between layers of the atmosphere, vertical diffusion, heat flux and frictional forces within the atmosphere. It also models the mixing of air between layers of the atmosphere (e.g., Hong and Pan 1996; Hong et al. 2006; Hong 2010; Gaines 2012). This scheme allows for the depth of the PBL to be determined from the thermal profile and a mixing scheme in the boundary layers and includes an explicit treatment of entrainment at the top of the PBL. This entrainment process leaves

more heat and moisture for the accurate representation of severe convection (Hong et al. 2006).

Kain–Fritsch cumulus convective parameterization (Kain 2004) includes convective trigger function and mass flux formulation and models updraft and downdraft, among others. This scheme is widely used in many model applications. WSM6 is a cloud microphysics parameterization scheme, which assumes that ice-phase processes primarily occur between 0° and −20°C. Rain and snow processes occur for temperatures above and below freezing, respectively. Ice crystal concentration is a function of ice amount (Dudhia 1989; Hong et al. 2004). These basic assumptions allow for a better distribution of cloud, ice, and snow concentrations. In short, WSM6 is the representation of different water forms including vapor, cloud water, cloud ice, rain, snow, and hail (Lin et al. 1983). For the simulations, 28 sigma levels were used.

## 2.2. Model domain, model performance, land cover, and model applications

This study has used a two-way nested domain setup where the outer domain encompassed the inland portion of the southeastern United States, spanning the near entirety of Kentucky and Tennessee and including portions of several surrounding states. Specifically, the outer domain has east–west bounds of 93.5° to 81.9°W longitude and north–south bounds of 32.3° to 39.9°N latitude (Figure 1). The inner domain included western Kentucky and Tennessee, with east–west extents of 89.7° to 86.5°W longitude and north–south bounds of 35.1°N to 37.7°N latitude (Figure 1). Within the inner domain, the LBL area has a 40-km east to west extent and 140-km north to south extent, spanning from 36.0° to 37.1°N latitude and 88.3° to 87.9°W longitude (Figure 1). The outer domain helped to capture meso- and synoptic-scale features, and an inner domain with higher resolution captured the finer details in the vicinity of the LBL. The outer and inner domains have spatial resolutions of 3 and 1 km, respectively.

Based on the U.S. Geological Survey (USGS) land-cover dataset, the inner domain is dominated by five land-cover types that include cropland/woodland mosaic, deciduous broadleaf forest, water bodies (i.e., LBL), dryland, cropland and pasture, and small areas of mixed forest (Figure 2). To determine impacts, we have modified the lake area to forest, grass, and bare soil.

This research uses North American Regional Reanalysis A (NARR-A; Mesinger et al. 2006) data from the National Centers for Environmental Prediction (NCEP; [http://nomads.ncdc.noaa.gov/data.php#narr\\_datasets](http://nomads.ncdc.noaa.gov/data.php#narr_datasets)). NARR-A data have a 32-km horizontal and 3-h temporal resolution. Three precipitation events of 22 September 2009, 23 August 2004, and 12 August 2013 were selected for this study. For each event, 36 h of NARR-A data were used starting at 0000 UTC on the first day (e.g., 22 September 2009, 23 August 2004, and 12 August 2013) and ending at 1200 UTC on the second day (e.g., 23 September 2009, 24 August 2004, and 13 August 2013). This allowed for 12 h of dynamic adjustment of the model before each of the precipitation occurrences.

The selection of these precipitation events for model sensitivity study was a multistep process. First, daily precipitation maps produced by the Advanced

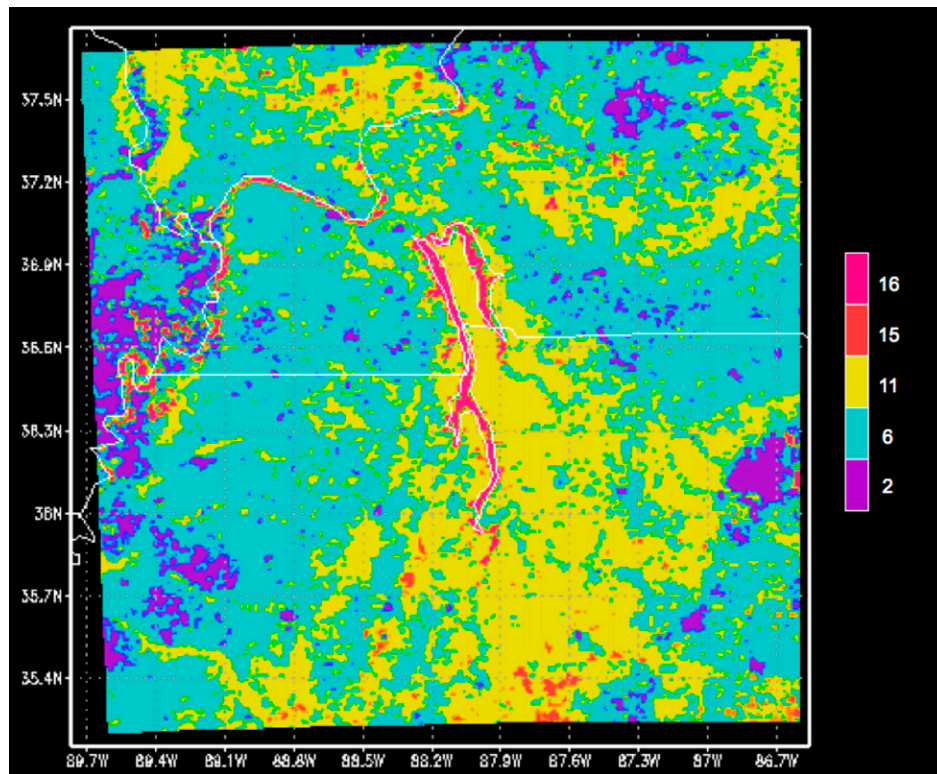


Figure 2. Land-use categories within the inner domain. These include dryland, cropland, and pasture (2, violet); cropland/woodland mosaic (6, cyan); deciduous broadleaf forest (11, yellow); mixed forest (15, red orange); and water bodies (16, magenta).

Hydrologic Prediction Service (AHPS) of the National Weather Service (NWS) were scanned to find days where there is precipitation occurring over the LBL area. For this purpose the warm-season (May–October) precipitation data from 2004 to 2013 were analyzed.

After selecting these days, a more specific analysis of daily precipitation was performed with archived radar imagery of the central Mississippi River valley from the University Corporation for Atmospheric Research (UCAR) and the National Center for Atmospheric Research (NCAR). This study has a focus on late warm-season convective episodes with relatively weaker synoptic circulation and forcing, especially when compared to early warm-season events. The timing of precipitation onset over the LBL was also noted for purposes of downloading the appropriate data files.

Subsequently, CTRL simulations of precipitation, temperature, and wind were compared to available observed (AHPS of the NWS) and reanalysis (NARR-A) data to assess model performance. AHPS data were not available for the pre-2005 period. As a result, we have compared 22 September 2009 and 12 August 2013 CTRL simulations with the AHPS data, and the 23 August 2004 CTRL simulation was compared to NARR data (Figures 3a–f).

F3

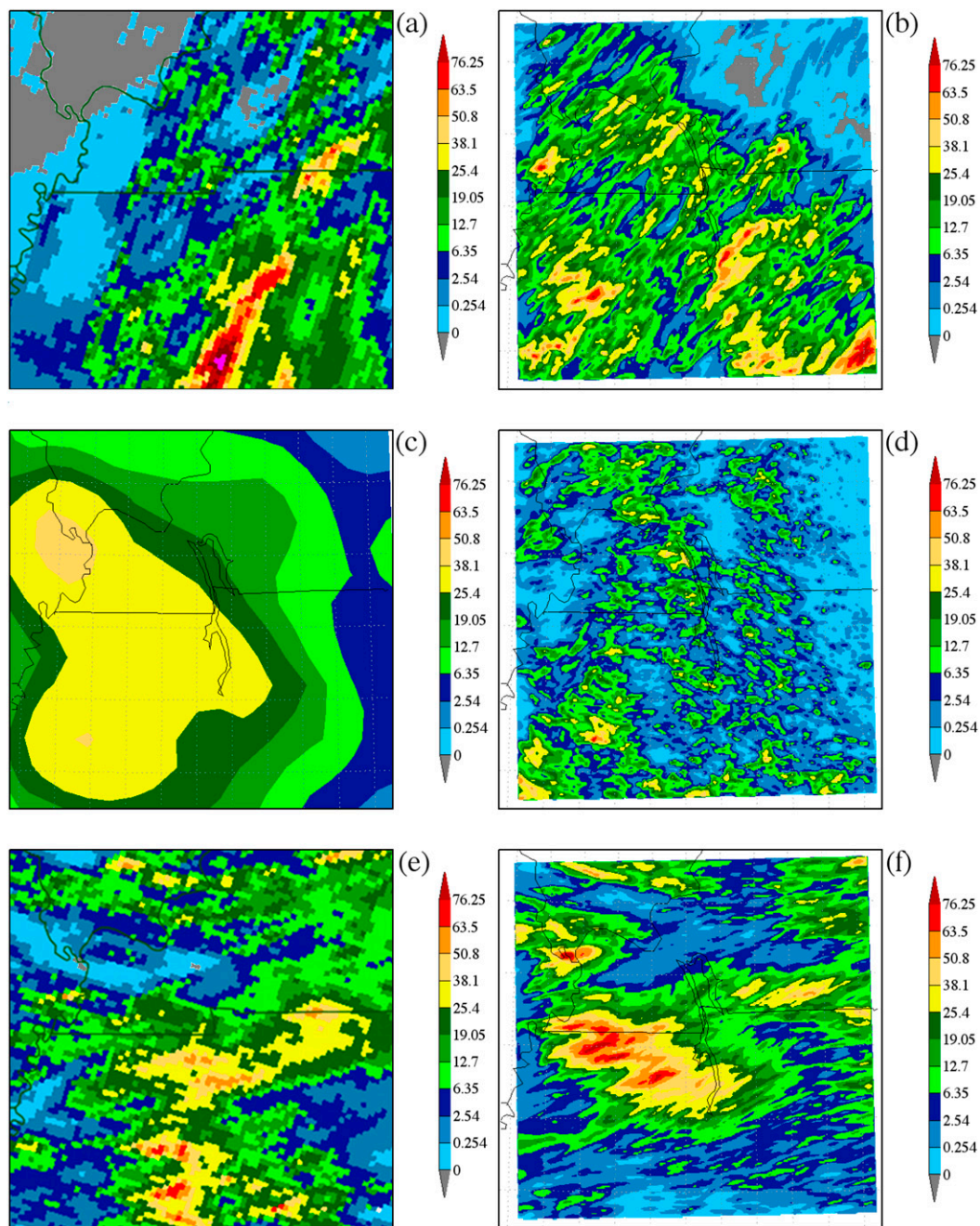


Figure 3. The 24-h accumulated precipitation (mm) within the inner domain starting at 1200 UTC for (a) AHPS data on 22 Sep 2009, (b) CTRL on 22 Sep 2009, (c) NARR-A on 23 Aug 2004, (d) CTRL on 23 Aug 2004, (e) AHPS data on 12 Aug 2013, and (f) CTRL on 12 Aug 2013. AHPS data are not available prior to 2005. The color schemes for CTRL precipitation here are different than rest of the CTRL figures below (Figures 4a and 13a) because they needed to be adjusted to AHPS data.

It is evident that the model generally captures distribution of 24-h accumulated precipitation for the 2009 and 2013 events. For example, like AHPS, for the 2013 event CTRL simulation shows higher precipitation around the central region of the inner domain (Figures 3e,f) and for the 2009 event CTRL captured higher precipitation in the southeastern quadrant of the domain (Figures 3a,b). For the 2004 event, the model showed generally higher precipitation in the western sector of the domain. We suggest that some of the discrepancy was linked to higher resolution of CTRL simulations (1 km) compared to lower resolution of AHPS (4 km) and NARR-A (32 km) data. Models have a general tendency of not matching location and or timing of precipitation. Based on CTRL simulations, however, it appears that the WRF did a fine job.

Inner domain 24-h average temperature for CTRL simulations for 2009, 2004, and 2013 events were 23.2°, 24.0°, and 24.7°C. NARR-A data-based temperatures for these events were 26.0°, 25.1°, and 25.6°C, respectively. In other words, the model had a tendency to underestimate temperatures (overall about 1.5°C), and we suspect that these were linked to simulated CTRL precipitation distribution and comparable to other studies in this region (e.g., Mahmood et al. 2011). However, it needs to be noted that the hourly temperature distribution for CTRL simulations were all in phase with NARR-A data.

Recall that the resolution of NARR-A data is 32 km, while the resolution of CTRL simulations for the inner domain was 1 km. As a result, the CTRL simulations produced much smaller-scale features of wind fields that were not visible in NARR-A data (not shown here). However, higher winds relative to some precipitation locations were reported. Moreover, the general distribution of winds in NARR-A data and CTRL simulations were comparable. For example, wind speeds for the 2009 event were higher in the southwestern quadrant of NARR-A data. Similar results can be found for CTRL simulation. Based upon model performance with respect to reanalysis data, CTRL simulations were able to reasonably capture these precipitation events.

In section 3, precipitation events (22 September 2009, 12 August 2013, and 23 August 2004) are not presented in chronological order. These are discussed based on the observed precipitation amounts. Based on the analysis of the observed data, the first event represents a moderate precipitation episode followed by relatively greater and lesser events. The event of 22 September 2009 was considered relatively moderate based on the analysis for warm-season data from 2004 to 2013, as noted above. Because of the unavailability and uncertainty in the data, we relied on the control model run to select the 23 August 2004 event (low precipitation). The rationale for the order of discussion is that it would allow us to systematically investigate the response of precipitation of different magnitudes (moderate/baseline, high, and low) and related variables to different land covers (GRAS, FORE, and BARE).

In addition to changes in precipitation under LULCC conditions, modifications in wind, latent heat (LH) and sensible heat (SH) fluxes, equivalent temperature  $\theta_e$ , PBL heights, and convective available potential energy (CAPE) were also discussed. Heat fluxes, for example, can impact atmospheric stability and play an important role in development (vertical expansion and contraction) of PBL and hence subsequent transfer and distribution of heat and moisture, development of convection, and potentially precipitation. The important roles of these variables in

convective development can be found in several key papers by Pielke (2001), Eltahir (1989), and Findell and Eltahir (2003), and evaluated in many similar studies such as Quintanar et al. 2008, Leeper et al. 2011, Mahmood et al. 2011, and Suarez et al. 2014.

Throughout the paper, results are presented in terms of inner domain and LBL area. These areas are shown by boxes b and c, respectively, in Figure 1. We have presented results for the LBL area so that atmospheric response in the immediate vicinity of the lakes and changed land uses can be identified and noted. In addition, for the sake of brevity, whenever appropriate we kept our discussion shorter for the second and the third precipitation events.

### 3. Results

#### 3.1. 22 September 2009: Moderate precipitation event

##### 3.1.1. Precipitation

On this day, a progressive northeast–southwest-oriented, upper-atmospheric trough axis was positioned across the upper Midwest into the central plains. At the surface, a low pressure center developed over southern Missouri in response to a shortwave impulse and, to a certain extent, in association with a remnant mesoscale convective vortex. These circulation features set the stage for two rounds of precipitation across the LBL area. The first round was associated with lift along a quasi-stationary surface boundary that transitioned to a poleward-advancing warm front. With the surface low just upstream in southern Missouri, the placement of LBL in the warm sector was limited. Consequently, an advancing cold front in association with maturing cyclogenesis induced the second round of precipitation.

Modeled accumulated precipitation for the control simulation (CTRL) in the 24 h after the 12-h spinup time showed that most precipitation occurred in the central LBL area on the order of 15–45 mm (Figure 4a). Changing the lakes to grassland (GRAS) in this event resulted in a decrease in accumulated precipitation in the central LBL by as much as 32 mm compared to CTRL. This is the same area that received the most precipitation in CTRL. The northern and southern extents of the area, however, experienced increases of up to 48 mm (Figure 4b). The decrease in greater precipitation areas and the increase of lesser precipitation areas imply a redistribution of rainfall between GRAS and CTRL. This result is in line with soil moisture sensitivity experiments conducted by Quintanar et al. (2008, 2009, 2012). Replacing water with broadleaf deciduous forest (FORE) increased precipitation for the already greater precipitation areas in the central LBL by up to another 48 mm, with isolated areas with greater amounts. This area of increased precipitation also extends somewhat into the southern LBL area as well. The northern LBL with its relatively lesser precipitation in CTRL experienced a further reduction in FORE of as much as 32–48 mm (Figure 4c). The patterns in FORE closely resembled BARE (replacing water with bare soil; Figure 4d).

Different spatiotemporal patterns emerged when we compared accumulated precipitation for four land-cover simulations. For the inner domain (Figure 1b), accumulated precipitation was highest for CTRL in the hours leading up to the main event (Figure 5a). While for GRAS simulation, precipitation was much lower.



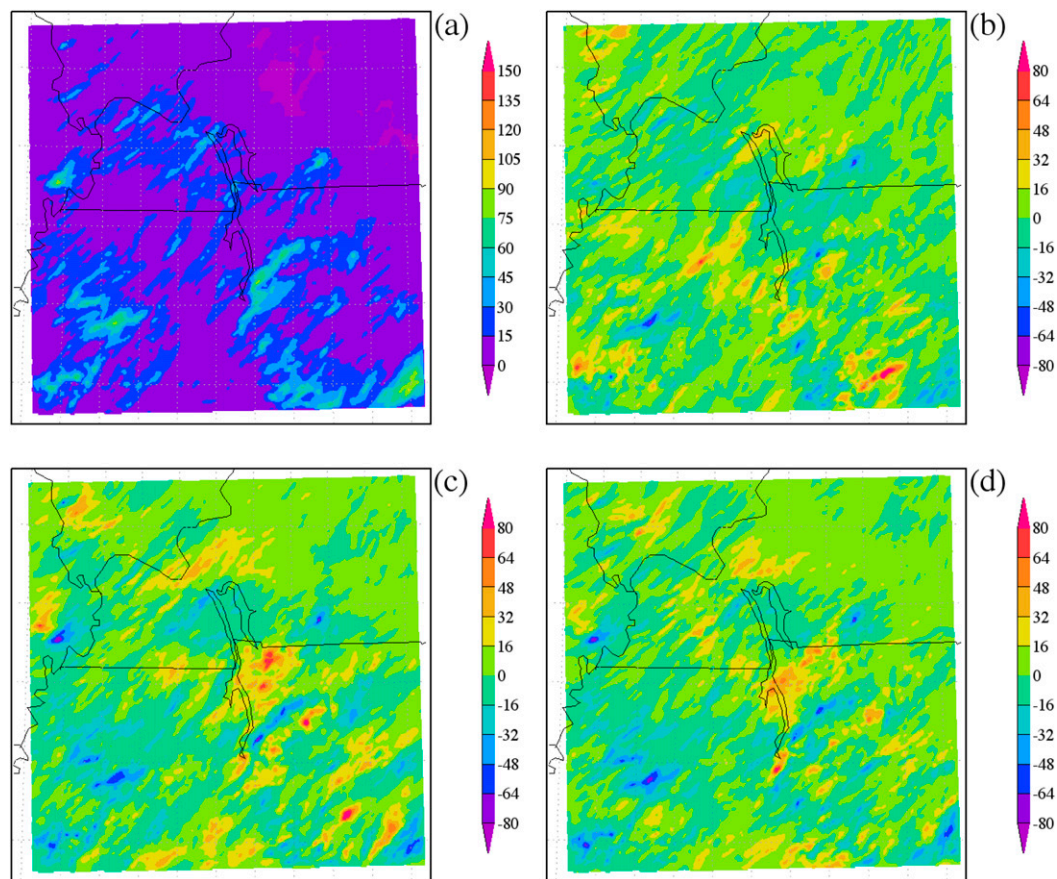


Figure 4. Accumulated precipitation (mm) for the inner domain from 1200 UTC 22 Sep 2009 to 1200 UTC 23 Sep 2009 for (a) CTRL, (b) GRAS-CTRL, (c) FORE-CTRL, and (d) BARE-CTRL. CTRL color scheme and scale shown in Figure 4a needed to be adjusted to Experiment-CTRL data.

It was also found that the changes in land cover led to changes in timing, location, duration, and amount of precipitation. For example, in the inner domain (Figure 1b), the main event (between 2000 and 0000 UTC) started about 2 h earlier and peaked about an hour later with slightly larger amounts in FORE and BARE than in GRAS and CTRL.

However, inner domain total precipitation totals for all simulations were in close agreement. By the end of this period, the GRAS simulation produced the most precipitation (11.92 mm), followed by CTRL (11.75 mm), FORE (11.62 mm), and BARE (11.36 mm; Figure 5a). In other words, key impacts of land over change (lakes versus forest, grass, bare soil) were not the domain total precipitation but rather the redistribution (including enhancement and reduction) of precipitation over time and space. Moreover, it is recognized that these small differences could be linked to model uncertainty.

For the LBL area (Figure 1c) and its immediate surroundings, precipitation began at 1500 UTC in all simulations and produced a quite similar amount until

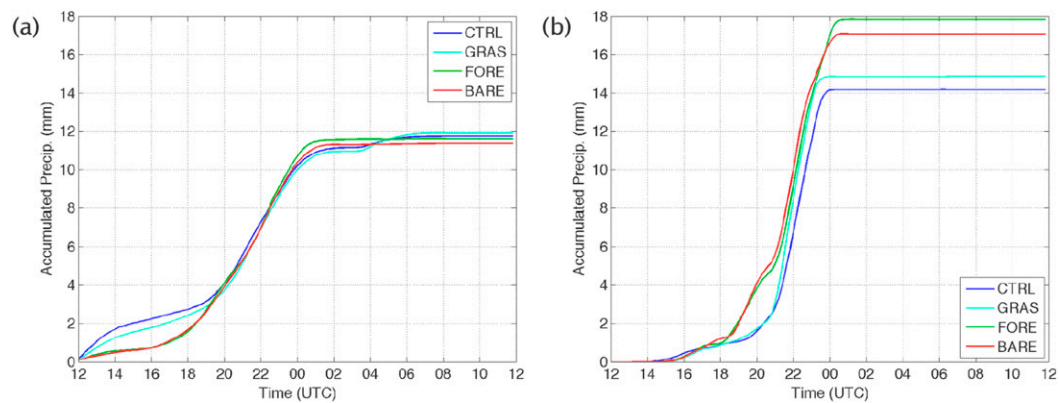


Figure 5. Accumulated precipitation (mm) for (a) the inner domain (box b in Figure 1) and (b) the LBL area (box c in Figure 1) in all simulations from 1200 UTC 22 Sep 2009 to 1200 UTC 23 Sep 2009.

1830 UTC (Figure 5b). By 0000 UTC 23 September, the FORE simulation produced the highest accumulated precipitation over the LBL area with 17.85 mm, followed closely by BARE with 17.08 mm. GRAS and CTRL were also in close agreement but with lower accumulation than the others, with 14.87 and 14.19 mm, respectively (Figure 5b).

### 3.1.2. Wind

In the CTRL simulation, the horizontal wind speeds were higher in or near to the location of precipitation. The highest speeds were estimated at 2200 UTC 22 September in the central LBL, exceeding  $16 \text{ m s}^{-1}$ . The northern and southern ends of the LBL had much calmer winds during this time (Figure 6a) for CTRL.

The winds in the GRAS simulation were not as high over the same area of the LBL as those in CTRL (Figures 6a,b), but higher winds of up to  $8 \text{ m s}^{-1}$  were present in the northern and southern ends (Figure 6b). These areas were close to or coincided with precipitation locations. Similarly, increases in wind speeds were found in the vicinity of precipitation in the LBL area for FORE and BARE simulations (Figures 6c,d). In the latter case, for example (BARE simulation), enhanced heating and larger sensible heat flux resulted in thermal instability and increased wind. This was accompanied by very low surface roughness length that also allowed stronger surface wind to develop. In addition, enhanced heating and increased sensible heat flux from BARE led to a deeper boundary layer. In a previous study, Mahmood et al. (2011) also demonstrated this chain of events and responses of surface wind and PBL.

### 3.1.3. Latent and sensible heat flux

Comparison of the LH from water in the CTRL to those of the GRAS, FORE, and BARE revealed distinct differences (Figures 7a–d). In CTRL at 2200 UTC 22 September, lake surfaces had LH below  $60 \text{ W m}^{-2}$  (Figure 7a). There was also low

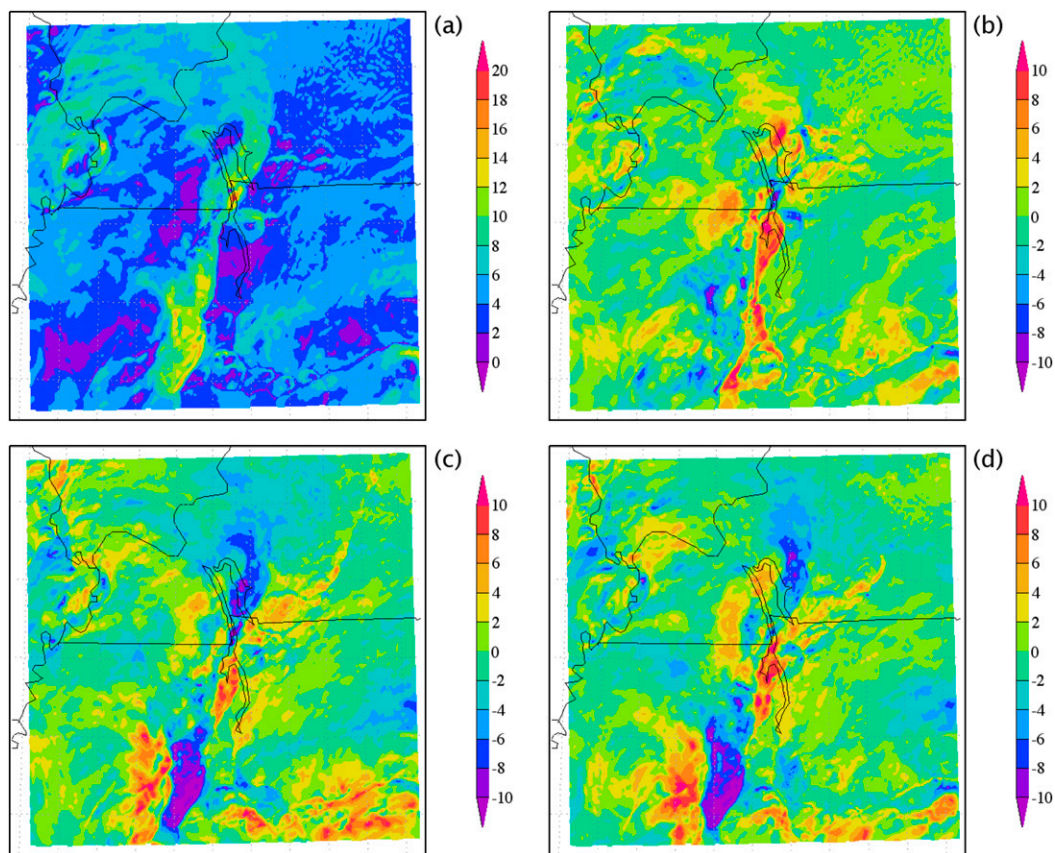


Figure 6. Horizontal wind speeds ( $\text{m s}^{-1}$ ) for the inner domain at 2200 UTC 22 Sep 2009 for (a) CTRL, (b) GRAS-CTRL, (c) FORE-CTRL, and (d) BARE-CTRL.

LH west of the lake at this time, which corresponded with the locations of precipitation in the model (Figure 7a). Changes of LH in GRAS showed increase up to  $240 \text{ W m}^{-2}$  in the southern half of the LBL, where precipitation had not occurred yet (Figure 7b). Similar increases in LH compared to CTRL were present in FORE (Figure 7c). LH increase in BARE over the lakes were more modest, averaging  $<100 \text{ W m}^{-2}$  compared to CTRL. In the forested portions of the central LBL, LH decreased in BARE by as much as  $80\text{--}160 \text{ W m}^{-2}$  (Figure 7d).

Sensible heat flux at 2200 UTC 22 September was downward for most of the lake areas and a portion of land area within the LBL area in the CTRL simulation. The remainder of the land area experienced positive SH of up to  $100 \text{ W m}^{-2}$  (Figure 8a). Negative fluxes were also present to the immediate west of the LBL where precipitation was heaviest at the time. Changes in sensible heat flux in the LULCC simulations were positive in all cases, with BARE simulating the largest increase, followed by FORE and then GRAS (Figures 8b–d).

Area-averaged sensible heat flux for the inner domain rose to near  $175 \text{ W m}^{-2}$  by 1800 UTC 22 September in CTRL and GRAS, while that for FORE and BARE was over  $190 \text{ W m}^{-2}$  at the same time (not shown). As expected, peak area-averaged sensible heat fluxes for the LBL area were lower than that of the inner domain

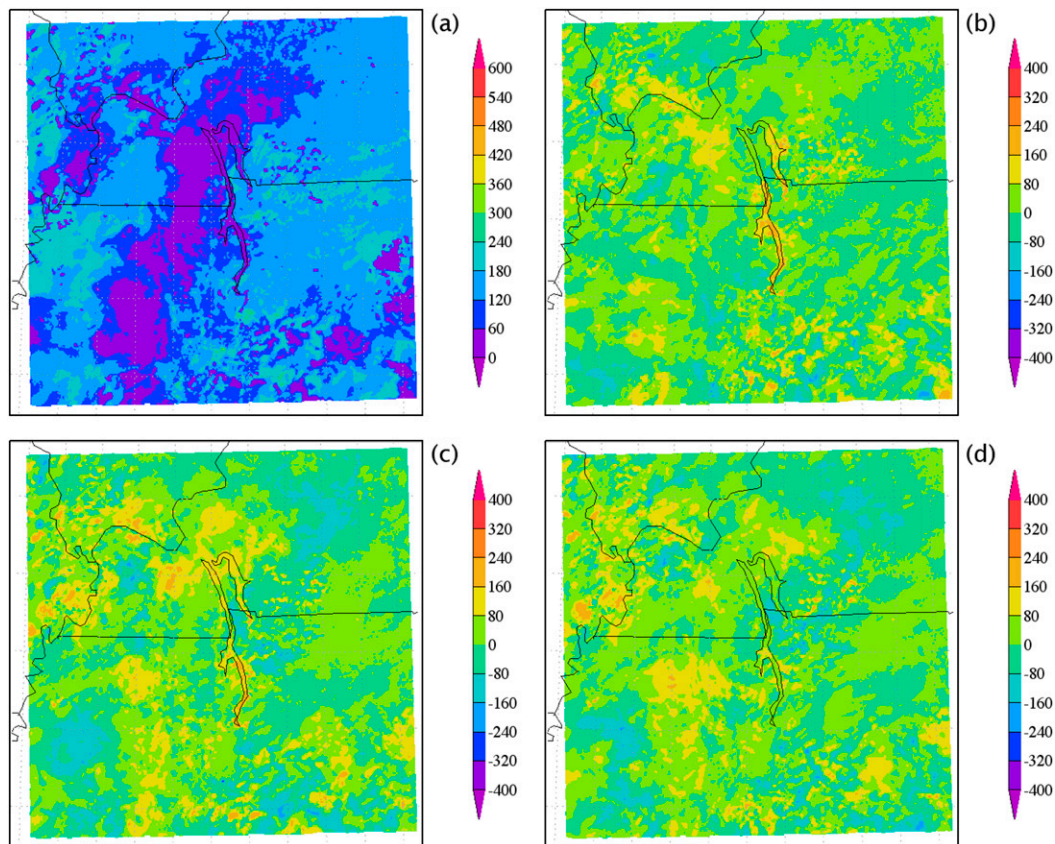


Figure 7. Latent heat flux ( $\text{W m}^{-2}$ ) for the inner domain at 2200 UTC 22 Sep 2009 for (a) CTRL, (b) GRAS-CTRL, (c) FORE-CTRL, and (d) BARE-CTRL.

average, ranging between  $155 \text{ W m}^{-2}$  for CTRL and  $170 \text{ W m}^{-2}$  for BARE (not shown).

### 3.1.4. Equivalent potential temperature $\theta_e$

To assess vertical distribution, we have analyzed modeled  $\theta_e$  for the surface, 850-, 700-, and 500-mb levels;  $\theta_e$  at the surface at 2200 UTC 22 September, ranged between 329 and 338 K in the northern half of the LBL area and areas to the west, corresponding with precipitation occurrence in CTRL (Figure 9a). In the southern and eastern half of the LBL area,  $\theta_e$  was higher, ranging between 338 and 344 K. Compared to CTRL, the GRAS simulation estimated an increase of up to 6 and 9 K for the southern and northern part of the LBL area, respectively (Figure 9b). FORE (Figure 9c) and BARE (Figure 9d) simulations reported similar spatial distribution of  $\theta_e$ .

At the 850-mb level,  $\theta_e$  was similar to that at the surface across a large portion of the inner domain and LBL area and ranged between 326 and 335 K. The southern half of the LBL area had  $\theta_e$  between 335 and 344 K in CTRL (Figure 10a). In GRAS (Figure 10b), there was a larger area of decrease of up to 12 K in  $\theta_e$  in the

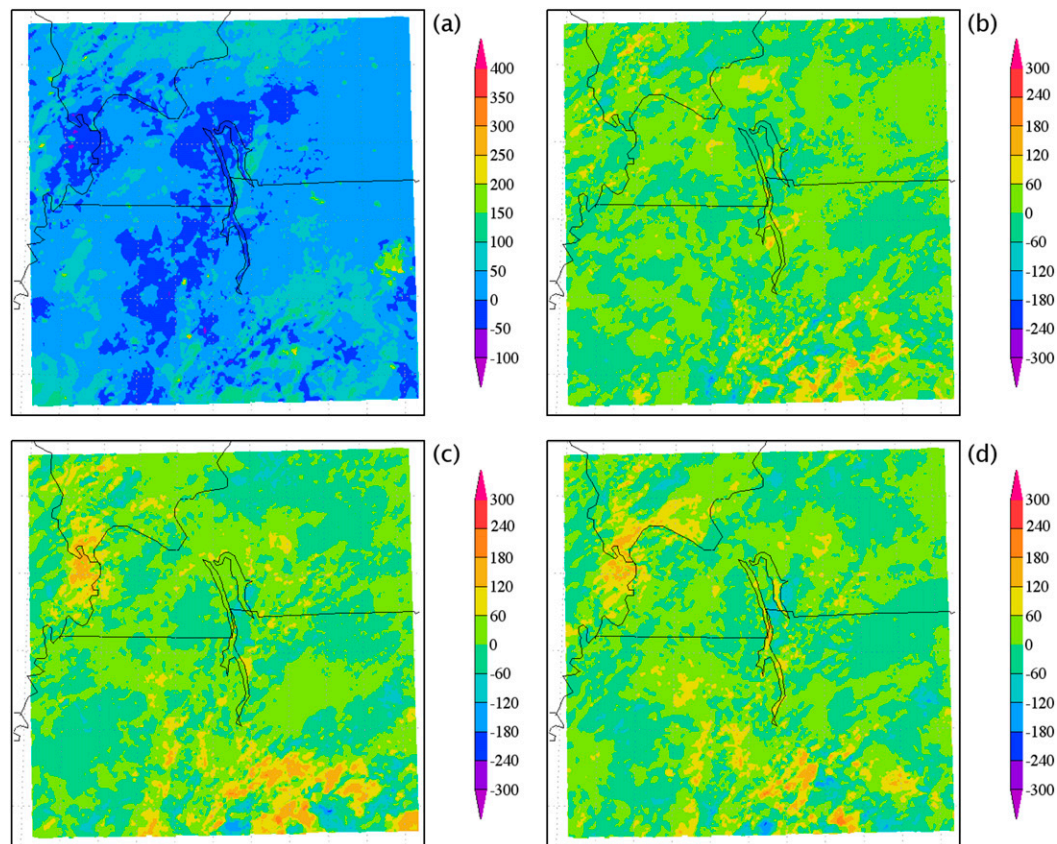


Figure 8. Sensible heat flux ( $\text{W m}^{-2}$ ) for the inner domain at 2200 UTC 22 Sep 2009 for (a) CTRL, (b) GRAS-CTRL, (c) FORE-CTRL, and (d) BARE-CTRL.

northeastern LBL and a significant increase of up to 15 K in the central LBL area. For FORE and BARE, we found increase in  $\theta_e$  in the northeastern part of the LBL area and less increase in the central part, compared to CTRL (Figures 10c,d).

At the 700- and 500-mb levels we found a band of higher  $\theta_e$  extending from the southwest to northwest, crossing the LBL area and closely coinciding with the precipitation bands. As expected, local  $\theta_e$  was up to 15 K higher than CTRL. However, these increases were not as widespread as those for the surface and 850-mb levels.

### 3.1.5. Planetary boundary layer height

The PBL height indicates strength of vertical mixing in the atmosphere and plays an important role in the development of convection and subsequent precipitation. PBL heights typically increase during the daytime and fall at night with decreasing fluxes and also with the onset of precipitation. It was found that PBL heights were low ( $<200$  m) in the areas of precipitation in CTRL at 2200 UTC including over the LBL and areas to west of the LBL. Areas east of the LBL had higher PBL heights exceeding 1200 m (not shown).

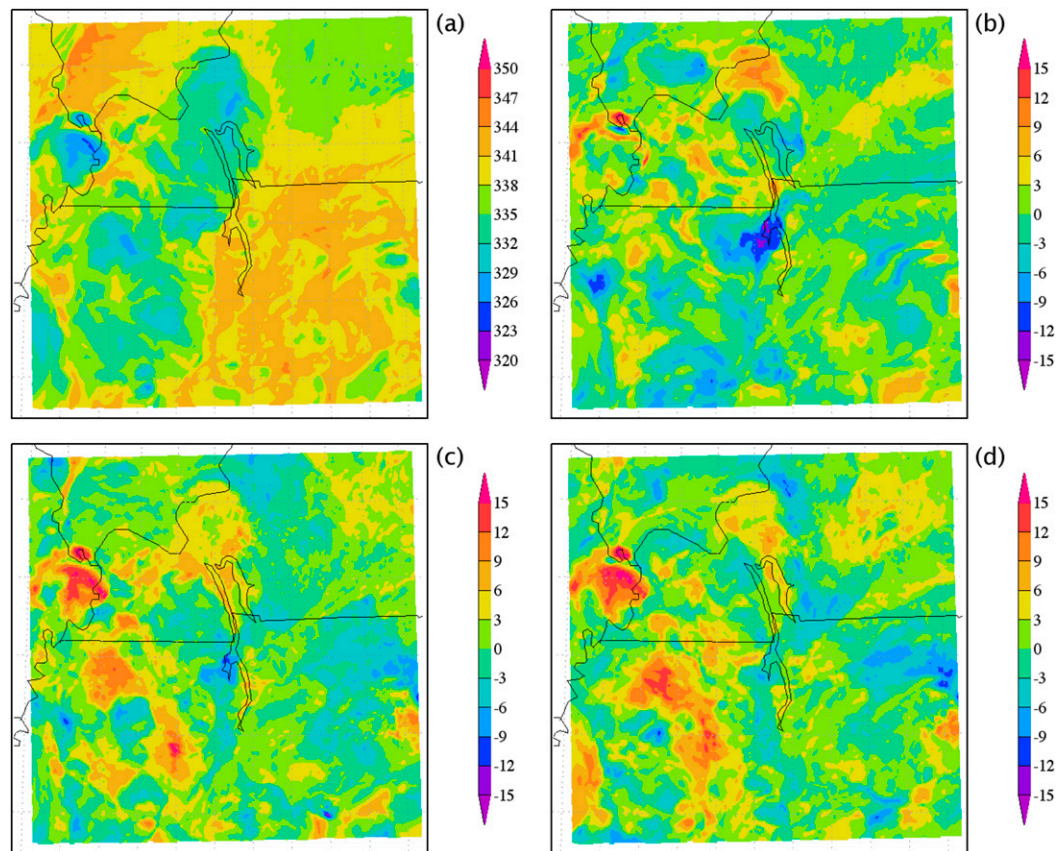


Figure 9. Equivalent potential temperature  $\theta_e$  (K) at the surface for the inner domain at 2200 UTC 22 Sep 2009 for (a) CTRL, (b) GRAS-CTRL, (c) FORE-CTRL, and (d) BARE-CTRL.

In the LBL area, PBL heights for the GRAS simulation were up to 600 m higher than those in CTRL, with most increases in the southern half. There were even greater height increases in the FORE (up to 900 m) over the southern half of the LBL area. Up to 1500 m increases in PBL height were found in BARE for the southern part of the LBL area.

Additionally, the CTRL and GRAS and FORE and BARE pairs show some similarity in the evolution of PBL height with time. By 1800 UTC, for the entire inner domain (Figure 11a), and by 1900 UTC, specifically for the LBL area (Figure 11b), PBL heights in the FORE and BARE simulations were up to 600 m higher than those in CTRL and GRAS. After the precipitation event at 2200 UTC, PBL heights fell for all simulations. FORE and BARE PBL heights remained higher than those in CTRL and GRAS by about 100–200 m.

### 3.1.6. Convective available potential energy

For the inner domain, CAPE had increased throughout the daytime hours in all simulations, peaking at between 1800 and 1900 UTC. However, BARE and FORE

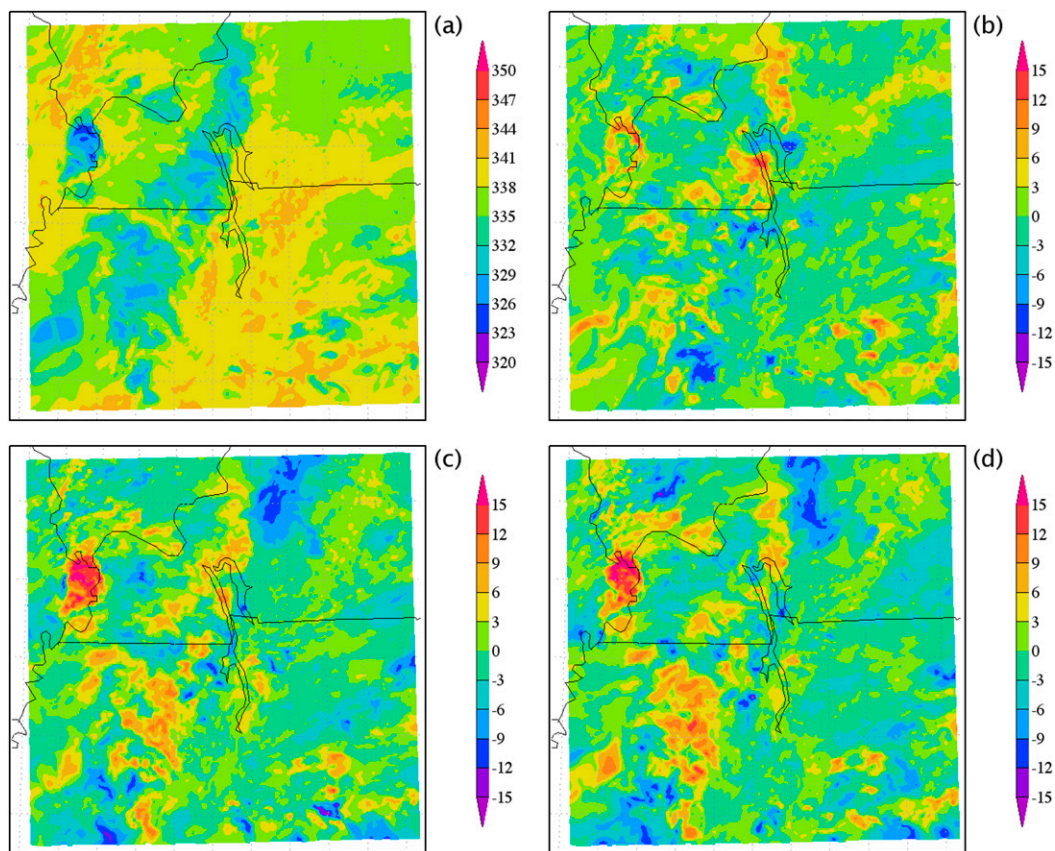


Figure 10. Equivalent potential temperature  $\theta_e$  (K) at the 850-mb level for the inner domain at 2200 UTC on 22 Sep 2009 for (a) CTRL, (b) GRAS-CTRL, (c) FORE-CTRL, and (d) BARE-CTRL.

had higher average CAPE with over  $1200 \text{ J kg}^{-1}$ , while CTRL and GRAS had over  $1100 \text{ J kg}^{-1}$  each (Figure 11c). With the onset of precipitation, CAPE declined in all simulations after 1900 UTC.

The timing of the peak in CAPE varied between simulations for the LBL area, where FORE and BARE peaking first at 1900 UTC followed by CTRL and GRAS after 2000 UTC. GRAS had the highest CAPE over the LBL, reaching near  $1300 \text{ J kg}^{-1}$ , on average (Figure 11d). Pre-precipitation increase in CAPE also suggests conditions conducive to convective activities and precipitation.

### 3.1.7. Moderate event summary

Overall for the inner domain, GRAS simulated the most precipitation while BARE simulated the least. Average LH was the highest in FORE and the lowest in CTRL. However, CTRL and GRAS had the highest average wind speed and FORE the lowest. This is likely due to the surface roughness differences between the land covers. During this event it was found that higher wind speeds were collocated with

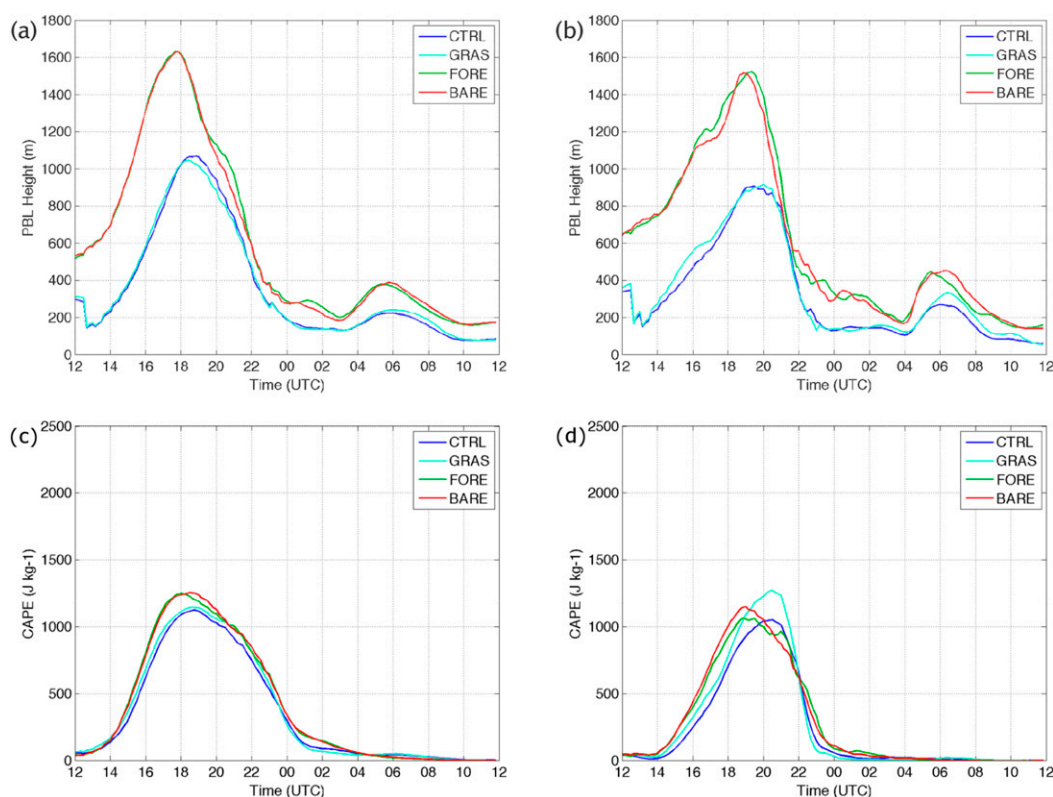


**Figure 11.** Average PBL height (m) for (a) the inner domain and (b) the LBL area in all simulations from 1200 UTC 22 Sep 2009 to 1200 UTC 23 Sep 2009 and average CAPE ( $\text{J kg}^{-1}$ ) for (c) the inner domain and (d) the LBL area in all simulations from 1200 UTC 22 Sep 2009 to 1200 UTC 23 Sep 2009.

areas of higher precipitation, suggesting increased local instability. It is also found that areas of increased  $\theta_e$  were collocated with nearby locations of increased precipitation;  $\theta_e$  is moist static energy (Pielke 2001) and hence influenced convection and precipitation. In other words, increased  $\theta_e$  near enhanced precipitation makes sense. Previously, Leeper et al. (2011), Mahmood et al. (2011), and Suarez et al. (2014) also showed  $\theta_e$  and its link to atmospheric moisture and precipitation in the current study region.

For the LBL area (Figure 1c), however, CTRL had the lowest accumulated precipitation, the lowest average latent heat flux, the lowest average PBL height, and the highest average wind speed. Meanwhile, FORE had the highest total precipitation, the highest average latent heat flux, the highest PBL height, the lowest average wind speed, and the highest surface roughness length. Physically, these estimates make sense because PBL height is the indication of PBL growth influenced by turbulent mixing. Together, the highest PBL height and latent energy flux suggest increase in potential for convective activities (e.g., Pielke 2001) and hence precipitation.

## 4. 12 August 2013 event: Larger precipitation event

### 4.1. Precipitation

On this day, a progressive northeast–southwest-oriented, upper-atmospheric trough axis was positioned across the upper Midwest, into the central plains. At the surface, a low pressure center developed over southern Missouri in response to a shortwave impulse and, to a certain extent, in association with a remnant mesoscale convective vortex. These circulation features set the stage for two rounds of precipitation across the LBL area. The first round was associated with lift along a quasi-stationary surface boundary that transitioned to a poleward-advancing warm front. With the surface low just upstream in southern Missouri, the placement of LBL in the warm sector was limited. Consequently, an advancing cold front in association with maturing cyclogenesis induced the second round of precipitation.

This event recorded the highest precipitation among the three. Within the inner domain, most of the rainfall in CTRL occurred west of the LBL area along the **F12** Kentucky–Tennessee border ( $>135$  mm; [Figure 12a](#)). The highest precipitation accumulation within the LBL area occurred in its southern half with 30–45 mm in most areas and a few locations exceeding 45 mm. The northern half of the LBL experienced less rainfall with less than 15 mm along the northern boundary of the LBL ([Figure 12a](#)). In GRAS, central LBL precipitation increased by up to 48 mm compared to CTRL, while the northern and southern ends of the LBL experienced rainfall reductions. This reduction was up to 32 mm in most areas ([Figure 12b](#)). These patterns imply a shift in location of precipitation in GRAS. The FORE simulation had a similar pattern, and magnitudes of differences were as those in GRAS with less than 20 mm in most areas ([Figure 12c](#)). A similar pattern of precipitation distribution was present in the BARE simulation. In addition, compared to FORE, a larger area of decreased precipitation in the southern LBL was found for BARE ([Figure 12d](#)).

Among simulations, accumulated precipitation started to differ noticeably in the inner domain after the first episode at 1230 UTC, with CTRL experienced the most **F13** precipitation by 1600 UTC, followed by FORE, BARE, and GRAS ([Figure 13a](#)). Accumulations for all simulations increased again during a second precipitation episode starting at 2200 UTC. FORE surpassed the others by 0400 UTC and reached 12.36 mm by the end of the simulation period. It was followed by CTRL, BARE, and GRASS with precipitation amount of 11.65, 11.64, and 11.16 mm, respectively ([Figure 13a](#)). These changes were within the model uncertainty.

For the LBL area ([Figure 1c](#)), most of the precipitation was received between 1200 and 1600 UTC. By the end of the model period, CTRL had the highest accumulated precipitation with 17.49 mm, followed by GRAS, FORE, and BARE with 16.42, 15.68, and 15.08 mm, respectively ([Figure 13b](#)). Precipitation accumulation through time for the inner domain and LBL area also captured changes for different land covers. Additionally, they also clearly show modifications in the timing of peak precipitation due to changes in land cover over the lake area.

### 4.2. Wind

The highest wind speeds ( $8\text{--}12\text{ m s}^{-2}$ ) occurred over the LBL area in the CTRL simulation. In all land-cover change simulations for this event, the higher wind

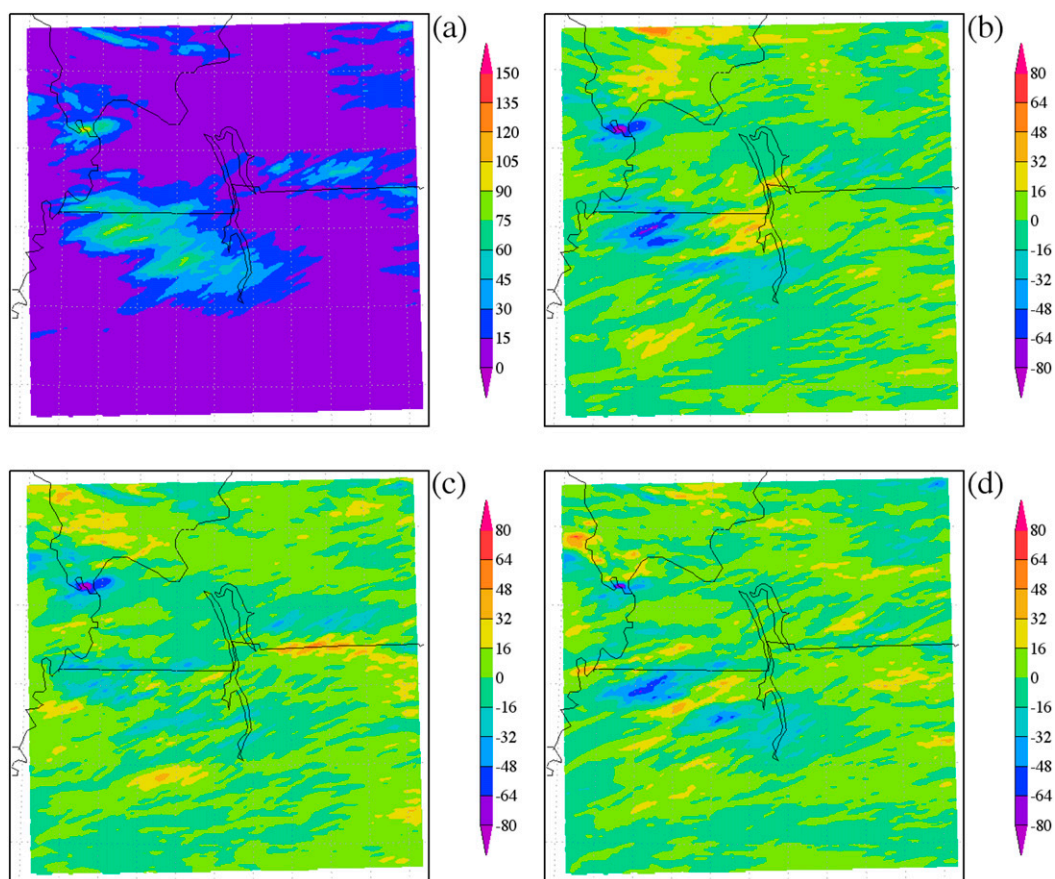


Figure 12. Accumulated precipitation (mm) for the inner domain from 1200 UTC 12 Aug 2013 to 1200 UTC 13 Aug 2013 for (a) CTRL, (b) GRAS-CTRL, (c) FORE-CTRL, and (d) BARE-CTRL. CTRL color scheme and scale shown in Figure 12a needed to be adjusted to experiment-CTRL data.

speeds of the central LBL were reduced by as much as  $6\text{--}8\text{ m s}^{-1}$ , with smaller reductions by up to  $2\text{ m s}^{-1}$  in the northern and southern ends of the LBL. Some of these changes can be attributed to the greater surface friction related to the LULCC. However, pockets of higher speeds can be found in the vicinity of increased precipitation cells suggesting conditions of instability.

### 4.3. Latent and sensible heat flux

Since this event occurred in the morning instead of the late afternoon or evening, LH over the lakes was higher than their surroundings. Specifically, LH in the northern LBL reached nearly  $500\text{ W m}^{-2}$ , in comparison to the surrounding fluxes of under  $60\text{ W m}^{-2}$ . Over the lakes (CTRL) LH flux was up to  $400\text{ W m}^{-2}$  higher compared to GRAS, FORE, and BARE. On the other hand, differences over land

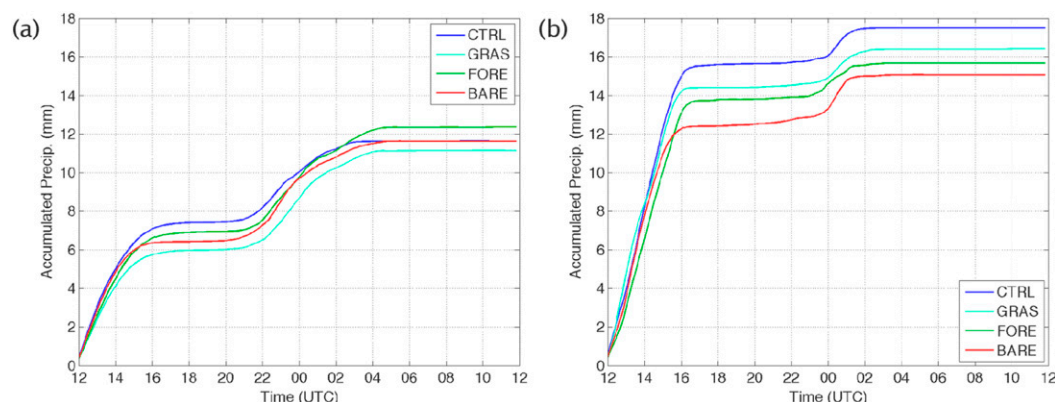


Figure 13. Accumulated precipitation (mm) for (a) the inner domain and (b) the LBL area in all simulations from 1200 UTC 12 Aug 2013 to 1200 UTC 13 Aug 2013.

areas experienced minimal change from CTRL. These illustrated the effects of the lakes (availability of water) on higher LH.

As expected, compared to CTRL, sensible heat fluxes were higher for LULCC simulations for the LBL area (box c in Figure 1) and over the lakes. Maximum fluxes for CTRL ( $190 \text{ W m}^{-2}$ ) and FORE ( $220 \text{ W m}^{-2}$ ) were reached at 1900 UTC. BARE ( $220 \text{ W m}^{-2}$ ) and GRASS ( $230 \text{ W m}^{-2}$ ) reached their maximum an hour earlier at 1800 UTC.

#### 4.4. Equivalent potential temperature

At the surface at 1230 UTC,  $\theta_e$  ranged between 326 and 335 K in the CTRL simulation. In the LULCC simulations, much of the change in  $\theta_e$  occurred along the leading edge of the precipitation across the central LBL area. In GRAS and BARE, there were increases from CTRL by up to 8 K, while in FORE, there was a small decrease.

At the 850-mb level,  $\theta_e$  was similar to that of the surface;  $\theta_e$  at the 700-mb level experienced localized increases up to 15 K extending to the west from the central LBL area and generally collocated with the areas of higher precipitation under LULCC simulations (not shown). At the 500-mb level,  $\theta_e$  increased from CTRL to the west of the central LBL area in all LULCC simulations, increasing by up to 3–8 K in FORE, GRAS, and BARE.

#### 4.5. Planetary boundary layer heights

At 1230 UTC and over the inner domain, PBL heights for CTRL were under 400 m over most of the lake areas while surrounded with much higher heights up to 1200 m for the adjacent land surfaces, especially to the east in the central LBL area (not shown). In all LULCC simulations, generally lower and higher PBL heights around the LBL area (900 m in both cases) were collocated with increased and decreased precipitation, respectively.

Overall, PBL heights for the inner domain for all simulations were quite similar for the 1230 UTC precipitation event and experienced lowering of about 150 m each. Simulations suggest that during peak development of PBL, CTRL had the shallowest depth and it was particularly visible around 2100 UTC. For the LBL area (box c on [Figure 1](#)), there were larger differences in PBL heights among simulations during 1230 UTC, with CTRL having the highest and FORE the shallowest, which resulted in largest differences for FORE–CTRL.

#### 4.6. Convective available potential energy

In the inner domain, CAPE from LULCC was generally up to  $1200 \text{ J kg}^{-1}$  higher than CTRL near to the locations/cells of increased precipitation at 1230 UTC. It was particularly true for GRASS and BARE. However, on average for the inner domain, CAPE was quite similar for all simulations during the 1230 UTC precipitation event and ranged between  $650$  and  $700 \text{ J kg}^{-1}$ . These values started to differ as the day progressed, with FORE reaching its peak near  $1750 \text{ J kg}^{-1}$  around 2200 UTC. For the LBL area and for all simulations, CAPE over the LBL area peaked later in the day (2300 UTC). Again, FORE had the highest CAPE at that time.

#### 4.7. Summary of larger precipitation event

CTRL (i.e., with the lakes) had the most precipitation within the LBL area, as well as the highest average LH and the lowest average PBL height. BARE experienced the least amount of rainfall in this area and also had the second lowest average LH and the second highest average PBL height. For the inner domain, GRAS experienced the lowest total precipitation and also had the highest average LH and PBL height.

### 5. 23 August 2004 event: Small precipitation event

#### 5.1. Precipitation

For this event, the LBL area was positioned just on the poleward side of a northwest/southeast surface quasi-stationary/warm frontal boundary that was largely derived from a broad, southerly, low-level moisture fetch from the Gulf of Mexico. Farther to the northwest, large-scale ascent was forced by the passage of a northwest–southeast-oriented midlevel shortwave across Missouri, collocated with the aforementioned advections, helped induce widespread convective development. In particular, scattered convective storms initially developed along the boundary across LBL. Later that evening, the southern extent of convective clusters over Missouri propagated along the surface boundary and brought forth the convective system through the LBL area.

In the inner domain and LBL area, CTRL precipitation was largely less than 15 mm. For GRAS, there were a few locations over the LBL area or in the vicinity, where precipitation increased up to 48 mm. Similar general changes were also found for FORE and to some degree for BARE. Under FORE, a  $>40$ -mm increase was found south of the LBL.



Compared to previous events, the accumulated precipitation amount was much smaller throughout the inner domain. After precipitation ended at 0100 UTC 24 August, FORE experienced the highest accumulated rainfall (5.73 mm) followed by CTRL (4.93 mm), BARE (4.92 mm), and GRAS (4.80 mm). For the LBL area, FORE, GRAS, BARE, and CTRL simulated 7.83-, 6.94-, 5.88-, and 5.19-mm precipitation, respectively.



## 5.2. Wind

Compared to CTRL, there were small changes in the wind speed for GRAS, FORE, and BARE, and differences were under  $2 \text{ m s}^{-1}$  over the LBL area. In the inner domain, overall wind speeds through time were fairly in agreement for all simulations up to 1930 UTC. Subsequently, wind speeds for different land cover slightly increased in the vicinity of precipitation (not shown). For the LBL area, as expected, overall wind speeds were different for each land cover.

## 5.3. Latent and sensible heat flux

LH at 1930 UTC for the lakes were up to  $180 \text{ W m}^{-2}$  in the CTRL simulation and  $400 \text{ W m}^{-2}$  lower compared to their immediate surroundings (e.g., forests). In GRAS, FORE, and BARE, where the lakes were replaced with the respective land uses, there were up to  $400 \text{ W m}^{-2}$  increases in LH. As expected, LH fluxes were greater for CTRL after 0000 UTC 24 August.

Sensible heat flux was near zero or negative over the water surfaces of the LBL area in CTRL, with positive values around the lakes of up to  $250 \text{ W m}^{-2}$ . Negative SH also occurred around precipitation cells to the west of the LBL area. SH increased up to  $240 \text{ W m}^{-2}$  where lakes were changed to land in GRAS, FORE, and BARE.

## 5.4. Equivalent potential temperature

At the surface,  $\theta_e$  was highest where precipitation occurred, just to the west of the LBL area, ranging between 344 and 347 K in CTRL, while the LBL area itself ranged between 338 and 344 K. A localized increase in  $\theta_e$  of about 9 to 12 K occurred to the west of the central LBL in GRAS, FORE, and BARE. At the 850-mb level,  $\theta_e$  in the west of the LBL in CTRL was as high as 344 K. Following the surface pattern, localized increases between 3 and 6 K can also be found in the central LBL for GRAS, FORE, and BARE. This distribution of  $\theta_e$  was also evident at 700-mb level, implying a relatively enhanced area of available moist static energy in the general vicinity of precipitation cells.



## 5.5. Planetary boundary layer heights

The PBL heights for the lakes in the CTRL simulation for this event were lower compared to most of the inner domain, similar to the pattern observed for the other precipitation events. Several locations of heights under 400 m existed just to the west of the LBL area, coinciding with precipitation cells. PBL heights over the lake areas in GRAS, FORE, and BARE were 300–900 m higher than in CTRL.

## 5.6. Convective available potential energy

Over most of the inner domain, CAPE in CTRL remained high during the precipitation event at 1930 UTC. The highest CAPE was to the west of the lakes, exceeding  $2700 \text{ J kg}^{-1}$  in several areas. CAPE for the lakes themselves ranged between  $1500$  and  $2400 \text{ J kg}^{-1}$  during this time. Compared to CTRL, higher CAPEs for LULCC experiments were located in the west of the central LBL ( $800$ – $2000 \text{ J kg}^{-1}$ ). Simulations suggest that, in the LBL area and by 1930 UTC, CTRL experienced the highest CAPE near  $1800 \text{ J kg}^{-1}$ , followed by GRAS, FORE, and BARE.

## 5.7. Summary of small precipitation event

Overall for the 23–24 August event, FORE had the highest total precipitation ( $5.73 \text{ mm}$ ) for the inner domain. On other hand, GRAS had the lowest with a total of  $4.80 \text{ mm}$ . Again, it is important that, instead of domain total amounts, we consider modification in precipitation distribution over the inner domain and related changes in wind, fluxes, CAPE, and PBL heights. These changes occurred due to the land-cover alterations over the lakes.

## 6. Discussion and conclusions

In this modeling study, we have investigated the potential influences of two nearby parallel artificial lakes and the replacement of these lakes with grasslands, deciduous forests, and bare soils. For this purpose, the WRF Model was applied for three warm-season precipitation events (moderate/average, large, and small) and for the above land-cover types. In addition, simulations with the lakes served as control runs. Hence, a total of 12 simulations were conducted to fulfill the objectives of this study. Modeled precipitation, wind, latent heat (LH) and sensible heat (SH) fluxes, equivalent temperature  $\theta_e$ , planetary boundary layer (PBL) heights, and convective available potential energy (CAPE) were analyzed. The results in this study largely support the observational findings in [Durkee et al. \(2014\)](#). Below we highlight the key findings.

### 6.1. Impacts on precipitation

Model simulations demonstrated that modifications in precipitation due to LULCC or under current conditions (i.e., lakes) are complex and nonlinear. The results also suggest that substitution of lakes with various land-cover types might lead to increase or decrease in precipitation. From the simulations, LULCC led to the displacement of precipitation cells, changes in local precipitation amount (rather than domain wide), and timing of precipitation. Domainwide and LBL area ([Figure 1c](#)) precipitation distribution over time also demonstrated these findings. In all experiments and under all three events, localized increases or decreases in precipitation were noted.

On the other hand, we suggest that the establishment of lakes may or may not increase precipitation amounts for all events. For the sake of simplicity or brevity,

we commonly aggregate/composite data over space (e.g., average precipitation over the inner domain or LBL area). However, in these cases, assessment of spatial variations within the regions provided us with a much improved understanding of land surface atmospheric interactions and the impacts of LULCC on precipitation. This is further supported by the findings that accumulated precipitation over the LBL area (Figure 1c) shows greater changes compared to domainwide estimates for all events. We suggest that the impacts of this large source of additional moisture are dependent on the interplay of a variety of precipitation-controlling variables.

Of the three precipitation events considered, the case of 12 August 2013 produced the highest observed precipitation, and model simulations also indicated that the enhancement of precipitation in the LBL area (and in the inner domain to some degree) was due to the lakes (CTRL simulation). Experiments found that CTRL produced the highest accumulated precipitation (17.49 mm) in the LBL area, followed by GRAS, FORE, and BARE with 16.42, 15.68, and 15.08 mm, respectively. For the other two precipitation events (average/moderate and low), the inner domain- and LBL area-accumulated precipitation totals were greater under LULCC experiments compared to CTRL (i.e., with the lakes). This also illustrates the complexity and nonlinearity of impacts. The observational study of Durkee et al. (2014) demonstrated that in some cases convection was enhanced around the LBL area or after they traversed the lakes. In other circumstances, convection dissipated after traversing the LBL area.

## 6.2. Precipitation and $\theta_e$

The analysis of the thermodynamic variables supports our conceptual understanding of their links to precipitation and land surface conditions (e.g., Pielke et al. 2001). This study finds locations of precipitation increases were also generally within the vicinity of increased  $\theta_e$  and CAPE. For the 22 September 2009 and 12 August 2013 events, we noted  $\theta_e$  through a deep layer extending up to the 500-mb level. As noted previously,  $\theta_e$  is the indicator of availability of moist static energy in the atmosphere and hence existence of a deep layer suggests favorable condition for convection and precipitation. It was also found that locations of precipitation changes associated with LULCC were accompanied by pockets of increased wind speeds suggesting instability in the lower atmosphere.

## 6.3. Precipitation, CAPE, energy fluxes, and PBL

The current study reports significant increase of CAPE and PBL height right before the commencement of precipitation events. These are indicative of atmospheric instability and strong convective mixing that are commonly linked to subsequent precipitation. The present study also found lower SH over the lakes for all cases. This is expected because of the availability of free water where more energy will be partitioned into latent. Moreover, LH was higher at night over the lakes, and this is consistent with our understanding that water bodies could be a source of continued LH fluxes even at night (Oke 1987; Quintanar et al. 2009).

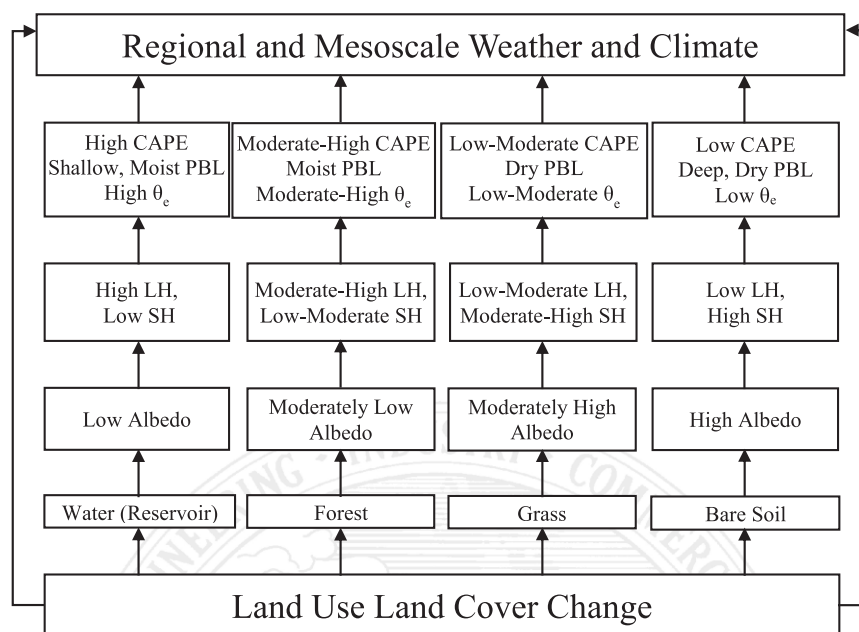


**Figure 14. An idealized and simplified conceptual model of impacts of water (man-made reservoir), forest, grass, and bare soil on regional and mesoscale weather and climate.**

These findings also point toward the question of what would be a preferable area/land cover that could be converted for man-made reservoir to minimize potential impacts. It is a complicated issue. Results from the present study suggest that the response of precipitation is nonlinear and space–time dependent. Precipitation under a particular land-cover type did not always provide the same type of response and was also dependent on an underlying meteorological condition.

However, when we introduce underlying climatological conditions in this discussion, a “clearer” scenario emerges. [Degu et al. \(2011\)](#), [Degu and Hossain \(2012\)](#), [Hossain \(2010\)](#), and [Hossain et al. \(2010\)](#) conducted detailed investigation on the impacts of man-made reservoirs on precipitation. They have considered dams from around the world including the United States (92 large dams). As noted in the introduction, they found that the modifications were mostly for summer precipitation over Mediterranean, semiarid, and arid climates ([Degu et al. 2011](#)) and increased the moistening of boundary layer by 5%–15% over areas downwind of dams ~~in the same regions during summer~~. Preliminary results suggest that postdam modification of surrounding land use land cover modifies/enhances precipitation ([Woldemichael et al. 2012, 2014a,b](#)). [Degu et al. \(2011\)](#) also noted that impacts on precipitation would be much less in the southeastern United States (study area for this research). Overall, in the context of our current understanding through the present study and the above research, impacts of reservoirs and other LULCCs on weather and climate can be presented as in [Figure 14](#). We suggest that additional modeling and observational data–based research needs to be completed before we begin policy recommendation.

In summary, this research suggests that as LULCC occurs, biophysical characteristics of the landscape also change. These changes alter land–atmosphere interactions via changing (by intensifying or moderating) physical process and various atmospheric measures. It is evident that these changes work through complex and nonlinear pathways to influence precipitation. For the events investigated here, there were no overwhelming physical processes that controlled precipitation. It was rather a combination of factors that impacted precipitation. Nonetheless, it is apparent that there was increased  $\theta_e$  through a deep vertical column of the atmosphere and wind speeds in the vicinity of precipitation. Moreover, there were increased PBL heights and CAPE prior to the precipitation. All of these are indicative of instability and strong vertical mixing in the atmosphere, leading to changes in precipitation.

However, further investigation is needed to conclusively identify impacts of LBL on precipitation. Based on the complexity and nonlinearity identified in this and the Durkee et al. (2014) study, a larger sample of events from different seasons and different underlying conditions, need to be selected where observational analysis can be complemented by modeling research. A similar approach could be applied for man-made lakes in other parts of the United States and the world (which would represent different hydroclimatic regimes) to further improve our understanding of the role of these lakes in local and regional weather and climate.

**Acknowledgments.** The authors thank two anonymous reviewers for their valuable comments and suggestions, which helped to improve this manuscript. This research **AU9** benefitted from a USDA Grant 58-6445-6-068.

## References

- Adegoke, J. O., R. A. Pielke Sr., J. Eastman, R. Mahmood, and K. G. Hubbard, 2003: Impact of irrigation on midsummer surface fluxes and temperature under dry synoptic conditions: A regional atmospheric model study of the U.S. high plains. *Mon. Wea. Rev.*, **131**, 556–564, doi:10.1175/1520-0493(2003)131<0556:IOIOMS>2.0.CO;2.
- , —, and A. M. Carleton, 2007: Observational and modeling studies of the impact of agriculture-related land use change on climate in the central U.S. *Agric. For. Meteorol.*, **142**, 203–215, doi:10.1016/j.agrformet.2006.07.013.
- Bates, B. C., Z. W. Kundzewicz, S. Wu, and J. P. Palutikof, 2008: Climate change and water. IPCC Tech. Paper, 210 pp.
- Betts, A. K., R. L. Desjardins, and D. Worth, 2007: Impact of agriculture, forest and cloud feedback on the surface energy budget in BOREAS. *Agric. For. Meteorol.*, **142**, 156–169, doi:10.1016/j.agrformet.2006.08.020.
- Carleton, A. M., J. Adegoke, J. Allard, D. L. Arnold, and D. J. Travis, 2001: Summer season land cover—Convective cloud associations for the Midwest U.S. “Corn Belt.” *Geophys. Res. Lett.*, **28**, 1679–1682, doi:10.1029/2000GL012635.
- Chang, J. T., and P. J. Wetzel, 1991: Effects of spatial variations of soil moisture and vegetation on the evolution of a prestorm environment: A numerical case study. *Mon. Wea. Rev.*, **119**, 1368–1390, doi:10.1175/1520-0493(1991)119<1368:EOSVOS>2.0.CO;2.
- Chen, F., and R. Avissar, 1994: Impact of land–surface moisture variability on local shallow convective cumulus and precipitation in large-scale models. *J. Appl. Meteorol.*, **33**, 1382–1401, doi:10.1175/1520-0450(1994)033<1382:IOLSMV>2.0.CO;2.

- , and J. Dudhia, 2001a: Coupling an advanced land surface–hydrology model with the Penn State–NCAR MM5 modeling system. Part I: Model implementation and sensitivity. *Mon. Wea. Rev.*, **129**, 569–604, doi:[10.1175/1520-0493\(2001\)129<0569:CAALSH>2.0.CO;2](https://doi.org/10.1175/1520-0493(2001)129<0569:CAALSH>2.0.CO;2).
- , and —, 2001b: Coupling an advanced land surface–hydrology model with the Penn State–NCAR MM5 modeling system. Part II: Preliminary model validation. *Mon. Wea. Rev.*, **129**, 587–604, doi:[10.1175/1520-0493\(2001\)129<0587:CAALSH>2.0.CO;2](https://doi.org/10.1175/1520-0493(2001)129<0587:CAALSH>2.0.CO;2).
- Clark, C. A., and R. W. Arritt, 1995: Numerical simulations of the effect of soil moisture and vegetation cover on the development of deep convection. *J. Appl. Meteor.*, **34**, 2029–2045, doi:[10.1175/1520-0450\(1995\)034<2029:NSOTEO>2.0.CO;2](https://doi.org/10.1175/1520-0450(1995)034<2029:NSOTEO>2.0.CO;2).
- Degu, A. M., and F. Hossain, 2012: Investigating the mesoscale impact of artificial reservoirs on frequency of rain during growing season. *Water Resour. Res.*, **48**, W05510, doi:[10.1029/2011WR010966](https://doi.org/10.1029/2011WR010966).
- , —, D. Niyogi, R. Pielke Sr., J. M. Shepherd, N. Voisin, and T. Chronis, 2011: The influence of large dams on surrounding climate and precipitation patterns. *Geophys. Res. Lett.*, **38**, L04405, doi:[10.1029/2010GL046482](https://doi.org/10.1029/2010GL046482).
- Dudhia, J., 1989: Numerical study of convection observed during the Winter Monsoon Experiment using a mesoscale two-dimensional model. *J. Atmos. Sci.*, **46**, 3077–3107, doi:[10.1175/1520-0469\(1989\)046<3077:NSOCOD>2.0.CO;2](https://doi.org/10.1175/1520-0469(1989)046<3077:NSOCOD>2.0.CO;2).
- Durkee, J., A. M. Degu, F. Hossain, R. Mahmood, J. Winchester, and T. Chronis, 2014: Investigating the effect of land between the lakes on storm patterns. *J. Appl. Meteor. Climatol.*, **53**, 1506–1524, doi:[10.1175/JAMC-D-13-088.1](https://doi.org/10.1175/JAMC-D-13-088.1).
- Eltahir, E. A. B., 1989: A feedback mechanism in annual rainfall, central Sudan. *J. Hydrol.*, **110**, 323–334, doi:[10.1016/0022-1694\(89\)90195-9](https://doi.org/10.1016/0022-1694(89)90195-9).
- Findell, K. L., and E. A. Eltahir, 2003: Atmospheric controls on soil moisture–boundary layer interactions. Part I: Framework development. *J. Hydrometeorol.*, **4**, 552–569, doi:[10.1175/1525-7541\(2003\)004<0552:ACOSML>2.0.CO;2](https://doi.org/10.1175/1525-7541(2003)004<0552:ACOSML>2.0.CO;2).
- Frye, J. D., and T. L. Mote, 2010: Convection initiation along soil moisture boundaries in the southern Great Plains. *Mon. Wea. Rev.*, **138**, 1140–1151, doi:[10.1175/2009MWR2865.1](https://doi.org/10.1175/2009MWR2865.1).
- Gaines, M., 2012: Application of the Weather Research and Forecasting (WRF) Model to simulate a squall line: Implications of choosing parameterization scheme combinations and model initialization data sets. M.S. thesis, ~~DEPT??~~  Western Kentucky University, 72 pp.
- Gangoiti, G., and Coauthors, 2011: Origin of the water vapor responsible for the European extreme rainfalls of August 2002: 1. High-resolution simulations and tracking of air masses. *J. Geophys. Res.*, **116**, D21102, doi:[10.1029/2010JD015530](https://doi.org/10.1029/2010JD015530).
- Gero, A. F., and A. J. Pitman, 2006: The impact of land cover change on a simulated storm event in the Sydney Basin. *J. Appl. Meteor. Climatol.*, **45**, 283–300, doi:[10.1175/JAM2337.1](https://doi.org/10.1175/JAM2337.1).
- Graf, W. L., 1999: Dam nation: A geographic census of American dams and their large-scale hydrologic impacts. *Water Resour. Res.*, **35**, 1305–1311, doi:[10.1029/1999WR900016](https://doi.org/10.1029/1999WR900016).
- Halldin, S., S.-E. Gryning, L. Gottschalk, A. Jochum, L.-C. Lundin, and A. A. Van de Griend, 1999: Energy, water and carbon exchange in a boreal forest landscape—NOPEX experiences. *Agric. For. Meteorol.*, **98–99**, 5–29, doi:[10.1016/S0168-1923\(99\)00148-3](https://doi.org/10.1016/S0168-1923(99)00148-3).
- Hong, S.-Y., 2010: A new stable boundary-layer mixing scheme and its impact on the simulated East Asian summer monsoon. *Quart. J. Roy. Meteor. Soc.*, **136**, 1481–1496, doi:[10.1002/qj.665](https://doi.org/10.1002/qj.665).
- , and H.-L. Pan, 1996: Nonlocal boundary layer vertical diffusion in a medium-range forecast model. *Mon. Wea. Rev.*, **124**, 2322–2339, doi:[10.1175/1520-0493\(1996\)124<2322:NBLVDI>2.0.CO;2](https://doi.org/10.1175/1520-0493(1996)124<2322:NBLVDI>2.0.CO;2).
- , and J.-O. Lim, 2006: The WRF single-moment 6-class microphysics scheme (WSM6). *J. Korean Meteor. Soc.*, **42**, 129–151.
- , J. Dudhia, and S. Chen, 2004: A revised approach to ice microphysical processes for the bulk parameterization of clouds and precipitation. *Mon. Wea. Rev.*, **132**, 103–120, doi:[10.1175/1520-0493\(2004\)132<0103:ARATIM>2.0.CO;2](https://doi.org/10.1175/1520-0493(2004)132<0103:ARATIM>2.0.CO;2).

AU10

- , Y. Noh, and J. Dudhia, 2006: A new vertical diffusion package with an explicit treatment of entrainment processes. *Mon. Wea. Rev.*, **134**, 2318–2341, doi:[10.1175/MWR3199.1](https://doi.org/10.1175/MWR3199.1).
- Hossain, F., 2010: Empirical relationship between large dams and the alteration in extreme precipitation. *Nat. Hazards Rev.*, **11**, 97–101, doi:[10.1061/\(ASCE\)NH.1527-6996.0000013](https://doi.org/10.1061/(ASCE)NH.1527-6996.0000013).
- , I. Jeyachandran, and R. Pielke Sr., 2010: Dam safety effects due to human alteration of extreme precipitation. *Water Resour. Res.*, **46**, W03301, doi:[10.1029/2009WR007704](https://doi.org/10.1029/2009WR007704).
- Iacono, M., J. Delamere, E. Mlawer, M. Shephard, S. Clough, and W. Collins, 2008: Radiative forcing by long-lived greenhouse gases: Calculations with the AER radiative transfer models. *J. Geophys. Res.*, **113**, D13103, doi:[10.1029/2008JD009944](https://doi.org/10.1029/2008JD009944).
- Jacquot, J., 2009: Dams, from Hoover to Three Gorges to the crumbling ones. *Discover*, 8 February. [Available online at <http://discovermagazine.com/2009/mar/08-dams-hoover-three-gorges-crumbling-ones>.]
- Kain, J., 2004: The Kain–Fritsch convective parameterization: An update. *J. Appl. Meteor.*, **43**, 170–181, doi:[10.1175/1520-0450\(2004\)043<0170:TKCPAU>2.0.CO;2](https://doi.org/10.1175/1520-0450(2004)043<0170:TKCPAU>2.0.CO;2).
- , and J. Fritsch, 1990: A one dimensional entraining/detraining plume model and its application in convective parameterization. *J. Atmos. Sci.*, **47**, 2784–2802, doi:[10.1175/1520-0469\(1990\)047<2784:AODEPM>2.0.CO;2](https://doi.org/10.1175/1520-0469(1990)047<2784:AODEPM>2.0.CO;2).
- AU11**  Kunstmann, H., and H. R. Knoche, 2011: Tracing water pathways from the land surface through the atmosphere: A new RCM-based evapotranspiration tagging method and its application to the Lake Volta region in West Africa. *Proc. Third iLEAPS Science Conf.*, Garmisch-Partenkirchen, Germany, ~~??SPONSOR??, xxx-xxx.~~ 
- AU12** Leeper, R., R. Mahmood, and A. I. Quintanar, 2011: Influence of karst landscape on planetary boundary layer atmosphere: A Weather Research and Forecasting (WRF) Model-based investigation. *J. Hydrometeor.*, **12**, 1512–1529, doi:[10.1175/2011JHM1260.1](https://doi.org/10.1175/2011JHM1260.1).
- LeMone, M. A., F. Chen, J. G. Alfieri, M. Tewari, B. Geerts, Q. Miao, R. L. Grossman, and R. L. Coulter, 2007: Influence of land cover and soil moisture on the horizontal distribution of sensible and latent heat fluxes in southeast Kansas during IHOP\_2002 and CASES-97. *J. Hydrometeor.*, **8**, 68–87, doi:[10.1175/JHM554.1](https://doi.org/10.1175/JHM554.1).
- Lin, Y., R. Farley, and H. Orville, 1983: Bulk parameterization of the snow field in a cloud model. *J. Climate Appl. Meteor.*, **22**, 1065–1092, doi:[10.1175/1520-0450\(1983\)022<1065:BPOTSF>2.0.CO;2](https://doi.org/10.1175/1520-0450(1983)022<1065:BPOTSF>2.0.CO;2).
- Mahmood, R., and K. G. Hubbard, 2002: Anthropogenic land use change in the North American tall grass-short grass transition and modification of near surface hydrologic cycle. *Climate Res.*, **21**, 83–90, doi:[10.3354/cr021083](https://doi.org/10.3354/cr021083).
- , R. Leeper, and A. Quintanar, 2011: Sensitivity of planetary boundary layer atmosphere to historical and future changes of land use/land cover, vegetation fraction, and soil moisture in western Kentucky, USA. *Global Planet. Change*, **78**, 36–53, doi:[10.1016/j.gloplacha.2011.05.007](https://doi.org/10.1016/j.gloplacha.2011.05.007).
- , and Coauthors, 2014: Land cover changes and their biogeophysical effects on climate. *Int. J. Climatol.*, **34**, 929–953, doi:[10.1002/joc.3736](https://doi.org/10.1002/joc.3736).
- McPherson, R. A., 2007: A review of vegetation–atmosphere interactions and their influences on mesoscale phenomena. *Prog. Phys. Geogr.*, **31**, 261–285, doi:[10.1177/0309133307079055](https://doi.org/10.1177/0309133307079055).
- , and D. J. Stensrud, 2005: Influences of a winter wheat belt on the evolution of the boundary layer. *Mon. Wea. Rev.*, **133**, 2178–2199, doi:[10.1175/MWR2968.1](https://doi.org/10.1175/MWR2968.1).
- , D. J. Stensrud, and K. C. Crawford, 2004: The impact of Oklahoma’s wheat belt on the mesoscale environment. *Mon. Wea. Rev.*, **132**, 405–421, doi:[10.1175/1520-0493\(2004\)132<0405:TIOOWW>2.0.CO;2](https://doi.org/10.1175/1520-0493(2004)132<0405:TIOOWW>2.0.CO;2).
- Mengelkamp, H.-T., and Coauthors, 2006: Evaporation over a heterogeneous land surface. *Bull. Amer. Meteor. Soc.*, **87**, 775–786, doi:[10.1175/BAMS-87-6-775](https://doi.org/10.1175/BAMS-87-6-775).
- Mesinger, F., and Coauthors, 2006: North American Regional Reanalysis. *Bull. Amer. Meteor. Soc.*, **87**, 343–360, doi:[10.1175/BAMS-87-3-343](https://doi.org/10.1175/BAMS-87-3-343).

- Nair, U. S., Y. Wu, J. Kala, T. J. Lyons, R. A. Pielke Sr., and J. M. Hacker, 2011: The role of land use change on the development and evolution of the west coast trough, convective clouds, and precipitation in southwest Australia. *J. Geophys. Res.*, **116**, D07103, doi:10.1029/2010JD014950.
- Narisma, G. T., A. J. Pitman, J. Eastman, I. G. Watterson, R. Pielke Sr., and A. Beltrán-Przekurat, 2003: The role of biospheric feedbacks in the simulation of the impact of historical land cover change on the Australian January climate. *Geophys. Res. Lett.*, **30**, 2168, doi:10.1029/2003GL018261.
- NCAR, 2012: WRF Model version 3.4.1: Updates. Accessed ~~xx-xxx-xxxx~~ available online at <http://www2.mmm.ucar.edu/wrf/users/wrfv3.4/updates-3.4.1.html>.]
- AU13** Oke, T. R., 1987: *Boundary Layer Climates*. 2nd ed. Methuen, 435 pp.
- Ookouchi, Y., M. Segal, R. C. Kessler, and R. A. Pielke, 1984: Evaluation of soil moisture effects on the generation and modification of mesoscale circulations. *Mon. Wea. Rev.*, **112**, 2281–2292, doi:10.1175/1520-0493(1984)112<2281:EOSMEO>2.0.CO;2.
- Pielke, R. A., Sr., 2001: Influence of the spatial distribution of vegetation and soils on the prediction of cumulus convective rainfall. *Rev. Geophys.*, **39**, 151–177, doi:10.1029/1999RG000072.
- Pielke, R. A., Sr., J. Adegoke, A. Beltrán-Przekurat, C. A. Hiemstra, J. Lin, U. S. Nair, D. Niyogi, and T. E. Nobis, 2007: An overview of regional land-use and land-cover impacts on rainfall. *Tellus*, **59B**, 587–601, doi:10.1111/j.1600-0889.2007.00251.x.
- , and Coauthors, 2011: Land use/land cover changes and climate: Modeling analysis and observational evidence. *Wiley Interdiscip. Rev.: Climatic Change*, **2**, 828–850, doi:10.1002/wcc.144.
- Quintanar, A. I., and R. Mahmood, 2012: Ensemble forecast spread induced by soil moisture changes over mid-south and neighbouring mid-western region of the USA. *Tellus*, **64A**, 17156, doi:10.3402/tellusa.v64i0.17156.
- AU14** —, —, J. Loughrin, and N. C. Lovanh, 2008: A coupled MM5-NOAH land surface model-based assessment of sensitivity of planetary boundary layer variables to anomalous soil moisture conditions. *Phys. Geogr.*, **29**, 54–78, doi:10.2747/0272-3646.29.1.54.
- , —, M. V. Motley, J. Yan, J. Loughrin, and N. Lovanh, 2009: Simulation of boundary layer trajectory dispersion sensitivity to soil moisture conditions: MM5 and Noah-based investigation. *Atmos. Environ.*, **43**, 3774–3785, doi:10.1016/j.atmosenv.2009.04.005.
- Schneider, N., and W. Eugster, 2005: Historical land use changes and mesoscale summer climate on the Swiss Plateau. *J. Geophys. Res.*, **110**, D19102, doi:10.1029/2004JD005215.
- Segal, M., and R. W. Arritt, 1992: Nonclassical mesoscale circulations caused by surface sensible heat flux gradients. *Bull. Amer. Meteor. Soc.*, **73**, 1593–1604, doi:10.1175/1520-0477(1992)073<1593:NMCCBS>2.0.CO;2.
- Sen Roy, S., R. Mahmood, A. Quintanar, and A. Gonzalez, 2011: Impacts of irrigation on dry season precipitation in India. *Theor. Appl. Climatol.*, **104**, 193–207, doi:10.1007/s00704-010-0338-z.
- Smith, E. A., M. M.-K. Wai, H. J. Cooper, and M. T. Rubes, 1994: Linking boundary-layer circulations and surface processes during FIFE 89. Part I: Observational analysis. *J. Atmos. Sci.*, **51**, 1497–1529, doi:10.1175/1520-0469(1994)051<1497:LBLCAS>2.0.CO;2.
- Suarez, A., R. Mahmood, A. I. Quintanar, A. Beltran-Przekurat, and R. A. Pielke Sr., 2014: A comparison of the MM5 and the Regional Atmospheric Modeling System simulations for land-atmosphere interactions under varying soil moisture. *Tellus*, **66A**, 21486, doi:10.3402/tellusa.v66.21486.
- Weaver, C. P., and R. Avissar, 2001: Atmospheric disturbances caused by human modification of the landscape. *Bull. Amer. Meteor. Soc.*, **82**, 269–282, doi:10.1175/1520-0477(2001)082<0269:ADCBHM>2.3.CO;2.
- Woldemichael, A. T., F. Hossain, R. Pielke Sr., and A. Beltrán-Przekurat, 2012: Understanding the impact of dam-triggered land use/land cover change on the modification of extreme precipitation. *Water Resour. Res.*, **48**, W09547, doi:10.1029/2011WR011684.

- , —, and R. A. Pielke Sr., 2014a: Evaluation of surface properties and atmospheric disturbances caused by post-dam alterations of land use/land cover. *Hydrol. Earth Syst. Sci.*, **18**, 3711–3732, doi:[10.5194/hess-18-3711-2014](https://doi.org/10.5194/hess-18-3711-2014).
- , —, and —, 2014b: Impacts of post-dam land use/land cover changes on modification of extreme precipitation in contrasting hydroclimate and terrain features. *J. Hydrometeor.*, **15**, 777–800, doi:[10.1175/JHM-D-13-085.1](https://doi.org/10.1175/JHM-D-13-085.1).
- Yan, H., and R. A. Anthes, 1988: The effect of variations in surface moisture on mesoscale circulation. *Mon. Wea. Rev.*, **116**, 192–208, doi:[10.1175/1520-0493\(1988\)116<0192:TEOVIS>2.0.CO;2](https://doi.org/10.1175/1520-0493(1988)116<0192:TEOVIS>2.0.CO;2).

---

*Earth Interactions* is published jointly by the American Meteorological Society, the American Geophysical Union, and the Association of American Geographers. Permission to use figures, tables, and *brief* excerpts from this journal in scientific and educational works is hereby granted provided that the source is acknowledged. Any use of material in this journal that is determined to be “fair use” under Section 107 or that satisfies the conditions specified in Section 108 of the U.S. Copyright Law (17 USC, as revised by P.L. 94-553) does not require the publishers’ permission. For permission for any other form of copying, contact one of the copublishing societies.

---

